

Library

BEATS BETWEEN TRANSVERSE MODES
IN A SAPPHIRE CLAD RUBY LASER

BEATS BETWEEN TRANSVERSE MODES
IN A SAPPHIRE CLAD RUBY LASER

By

KENNETH OWEN HILL, B.Eng.

A Thesis

Submitted to the Faculty of Graduate Studies
in Partial Fulfilment of the Requirements
for the Degree
Master of Engineering

McMaster University

May 1965

MASTER OF ENGINEERING (1965)
(Electrical Engineering)

McMASTER UNIVERSITY
Hamilton, Ontario

TITLE: Beats Between Transverse Modes in a Sapphire
Clad Ruby Laser

AUTHOR: Kenneth Owen Hill, B.Eng. (McMaster University)

SUPERVISOR: Dr. C. K. Campbell

NUMBER OF PAGES: vi, 97

SCOPE AND CONTENTS:

Experimental evidence is presented that supports the theory that beats between transverse modes are responsible for the fast modulation carried on occasions by laser relaxation oscillations.

ACKNOWLEDGEMENTS

It is with great pleasure that I take this opportunity to thank Dr. C. K. Campbell for his guidance and encouragement. I am particularly indebted to him for the many hours that he spent with me exploring the problems and possibilities which arose during my work on this thesis project.

My thanks go also to Mr. Derwyn Johnson for giving freely both of his time and of his knowledge of lasers.

TABLE OF CONTENTS

CHAPTER 1

INTRODUCTION

Section Number		Page Number
1.1	Resonant Modes in Laser Cavities	1
1.2	Scope of This Thesis	6

CHAPTER 2

RESONANT MODES IN A MASER INTERFEROMETER

2.1	Survey of the Work of A. Fox and T. Li	9
2.2	Solution of the Integral Equation for Circular Plane Mirrors	17
2.3	Equation for the Beats Between Transverse Modes	21

CHAPTER 3

EVIDENCE FOR EXISTENCE OF TRANSVERSE MODES

3.1	Brief Survey of Stickley's Work	23
3.2	Modes in Dielectric Optical Waveguides	25

CHAPTER 4

DESCRIPTION OF APPARATUS

4.1	Laser Head and Power Supply	30
4.2	Mounting	36
4.3	Detectors	36
4.4	Electronics	47
4.5	Experimental Arrangement	53

TABLE OF CONTENTS (CONTINUED)

CHAPTER 5

EXPERIMENTAL METHOD

5.1	Selection of the Sapphire Clad Ruby	55
5.2	Cooling of Sapphire Clad Ruby Crystal	60
5.3	Experimental Criteria	63
5.4	Photographic Synchronization Techniques	69
5.5	Formation of the Optical Cavity by Vacuum Deposition of Silver on the Crystal End Faces	72

CHAPTER 6

RESULTS		76
---------	--	----

CHAPTER 7

CONCLUSIONS		86
-------------	--	----

APPENDIX

A.	Confocal Mirror Cavity Equation	87
B.	Approximate Solution to the Coupled Non-linear Differential Equations of Galanin	92
REFERENCES		96

LIST OF ILLUSTRATIONS

Figure Number		Page Number
2.1	Geometry for the Rectangular Plane Parallel Laser Cavity	10
4.1	The Elliptical Laser Head	32
4.2	The Laser Power Supply	33
4.3	The Laser Head and External Mirror Holder Mounted on the Lathebed	35
4.4	Two Types of Diode Optical Detectors Capable of a Fast Response Time	37
4.5	An Optical Signal Detector Unit	38
4.6	Geometry Used to Calculate the Effect of Detector Tilt on the Beat Frequency Output	44 b
4.7	The Wide Band Amplifier	49
4.8	Schematic Diagram of the Beat Frequency Detection Apparatus	53 b
5.1	The Clad Ruby in the Holder	56
5.2	The Camera Used to Record the Beat Frequencies	71
5.3	A Precision Mirror Holder	73
6.1	Observed Beat Frequency Spectrum for a Cavity Diameter = $34/1000''$	77
6.2	Observed Beat Frequency Spectrum for a Cavity Diameter = $67/1000''$	78
6.3	Observed Beat Frequency Spectrum for a Cavity Diameter = $38/1000''$	79
6.4	Observed Beat Frequency Spectrum for a Cavity Diameter = $50/1000''$	80
6.5	Oscilloscope Traces Showing the Modulation Carried by Laser Relaxation Spikes	81
6.6	Oscilloscope Traces Showing the Modulation Carried by Laser Relaxation Spikes	82
6.7	Beat Frequency - Diameter Relationship for Low Order Modes	83

CHAPTER 1

INTRODUCTION

1.1 Resonant Modes in Laser Cavities

Modes occur often in the mathematical description of physical phenomena. Thus by the modes of a string of length L , which is constrained to remain motionless at two end supports, is meant the natural configurations that the string can take when it is allowed to go into a state of motion. The condition invoked is simply that an integral number of half wave lengths exist between the two supports along the string.

Thus the displacement
$$U_n(x,t) = A_n(t) \sin\left(\frac{n\pi x}{L}\right)$$
 describes the standing wave pattern on the string for each of the natural modes given by $n = 1, 2, 3 \dots$. If the string is initially displaced in an arbitrary fashion the arbitrary displacement can be expressed quite generally as an infinite sum of these natural modes of oscillation thus:

$$f(x,t) = \sum_{n=1}^{\infty} A_n(t) \sin\left(\frac{n\pi x}{L}\right)$$

When the string is released from its initial arbitrary displacement its motion can be determined by considering the motion of each natural mode of oscillation and then obtaining the net effect by simple summation of the individual motions of each of the modes.

In a lossy system different modes will be characterized by different loss rates so after a number of oscillations the resultant motion would be predominantly due to a few of the less lossy modes of oscillation.

Modes form in general a complete orthogonal set in the mathematical sense. In the physical sense the statement implies that if a system is oscillating in a particular mode it will remain in that mode as time develops. Each mode develops independently of the others.

The vibrating string is a one dimensional example of modes. We can think of the vibrating rectangular diaphragm as an extension of the problem into two dimensions and the argument is parallel to that for the one dimensional case considered. In three dimensions modes of oscillation can be associated in a similar manner with a rectangular volume of material.

Modes are of course not restricted to mechanical displacements or deformations. They are associated with physical systems that can be described within the framework of a mathematical model characteristic of wavelike motion. Thus wave guides exhibit modes of propagation. Wave mechanical systems are characterized by a wave-like probability function with which are associated discrete indices to represent different states of the system, the so-called stationary states. Finally, laser oscillators exhibit modes of oscillation.

The modes characteristic of laser oscillators are inherently three-dimensional, and are correspondingly characterized by three mode indices. Each index is used to describe in a qualitative fashion the way in which the electromagnetic energy is stored in the cavity. It is thus easy to obtain a qualitative picture of the electromagnetic field distribution knowing the mode indices of the field. The longitudinal index describes the number of half wavelengths of the light that are necessary to make up the length of the laser cavity. Thus $n \frac{\lambda}{2} = b$,

where n is in this case the longitudinal index, b the length of the cavity and λ is the wavelength of the electromagnetic field which is related to the free space wavelength λ_0 by $\lambda_0 = \mu\lambda$ where μ is the index of refraction of the medium. The above relationship is of course true only when the dimensions of the cavity are large compared with the free space wavelength of the electromagnetic energy being considered. The dimensions of the cavity will in general, through their constraining action, perturb the free space wavelength. The strength of the perturbation will be dependent on some ratio of wavelength and cavity dimensions.

That this ratio does indeed exist will be proved at a later stage. In particular it will be shown that the Fresnel number $\frac{a^2}{b\lambda}$ is the dimensionless variable that determines the perturbation in optical resonators of practical dimensions.

a - measure of the lateral dimension of the cavity

b - length of the cavity

λ - wavelength of the oscillation in the medium within the cavity.

The perturbation is small for practical cavities.

The transverse indices are employed to label in a qualitative fashion the number of nodes that the electromagnetic field goes through within the transverse dimensions of the cavity. Thus for a rectangular cavity the field will be TEM_{npq} where n is the longitudinal index, p is the transverse index for the x -dimension and q is the transverse index for the y -dimension. The transverse mode exhibiting no zeros in the transverse plane except perhaps at the boundaries of the plane (which is associated with the longitudinal index n), could be labelled TEM_{n00} . If a

single change in sign were exhibited in the x direction the corresponding label could be TEM_{n10} .

A laser oscillator is capable of amplifying radiation when a state of population inversion exists between two levels of the active medium. The electromagnetic energy amplified will have a frequency given by the expression $\Delta E = \hbar \omega$, where \hbar is Planck's constant and ΔE is the difference in energy between the two levels being considered. There is an inherent uncertainty in any measurement of ΔE arising from fundamental considerations. Any measurement of ΔE will be uncertain by an amount $d(\Delta E)$ such that $d(\Delta E) dt \geq \hbar$. dt here is the length of time taken to measure ΔE and is of the order of the lifetime of the state exhibiting the population excess. Since the lifetime of the state is finite, there will be a corresponding widening of the "sharp" transition due to the action of the uncertainty principle. This effect plays a negligible role in the width of the R_1 fluorescent line width of ruby. Lattice defects and phonon interaction play the major role.

The width of the R_1 fluorescent line of ruby is thus finite and easily measurable. Therefore ruby exhibiting a population excess between the 2E level and the 4A_2 ground state is capable of amplifying radiation within the line width of the R_1 fluorescence. This line width is typically 11 cm^{-1} at room temperature and is 0.3 cm^{-1} at 77°K .¹ A gain profile as a function of frequency would to a first approximation be given by the fluorescent line shape as a function of frequency.

A simple arithmetic computation shows that many longitudinal modes are capable of being amplified within the line width of the material

at room temperature, but this number is reduced considerably by operating the laser at liquid nitrogen temperatures.

Number of modes at room temperature for $1\frac{1}{2}$ " ruby = 84

Number of modes at 77°K for $1\frac{1}{2}$ " ruby = 3

Now, associated with each longitudinal mode of a given index are many satellite transverse modes whose frequency is slightly different from the fundamental longitudinal frequency. These transverse modes will also oscillate.

With so many close-lying modes the question of fundamental importance to this thesis is whether or not these transverse modes will be resolved in an active laser interferometer. Will the output of a laser exhibit the discreet frequencies of the various transverse and longitudinal modes? At the outset of the investigation it was known that high speed photography of the near and far field patterns of a laser oscillator showed the existence of definite patterns that could be unmistakably identified as being due to transverse modes.^{2,3,4,5} Also, high speed streak photography had shown a fast (30 - 40Mc) modulation of the output beam of ruby lasers.⁶ This modulation was attributed by Stickley⁷ to be due to transverse modes when he observed the same modulation using electronic detecting techniques.

Longitudinal modes had been shown to exist by time resolved spectroscopical techniques and microwave detection techniques, and have now been observed directly in Q-spoiled lasers using extremely fast detectors and associated circuitry. The observed beat frequency between adjacent longitudinal modes has agreed well with the predicted

$$\text{separation } \Delta f = \frac{nc}{2\mu L}$$

$$n = 1, 2, 3, 4 \text{ ---}$$

1.2 Scope of this thesis

This thesis will outline the theoretical work that has been done on the modes, by considering the models employed. Roughly speaking the work is initiated from two points of view, namely the solution of Maxwell's equations for dielectric clad optical fibres and the solution of an integral equation arising from the Fresnel field integral when the latter is used to describe the electromagnetic field in a laser interferometer.

Primary consideration will be given to the experimental techniques employed to observe the beat frequencies between transverse modes in a clad ruby laser oscillator. The results of measurements on the beat frequencies will be given and shown to correspond to the frequencies expected from a resonator of the dimensions used.

A method of solving the integral equation associated with a confocal cavity resonator will be given. Application of the method to the equation is original. The solutions obtained are valid in the high loss region. Low loss region solutions are available in the literature⁸ as are the high loss region solutions.⁹ However it is felt that the method presented expresses the solution in a practical form and this, together with the relative simplicity of its application, makes it worth while. An outline of the method will be found in the appendix of this thesis.

A specific set of laser rate equations will also be solved. The solution could prove useful for future research on relaxation oscillations.

It was pointed out in a previous section that the point of primary importance to this project was whether or not the transverse modes of the active Fabry Perot resonator are resolved. Longitudinal modes had been resolved by the incontestable method of spectroscopy. The resolution of state of the art spectroscopes is more than ample to resolve light separated in frequency by the order of gigacycles. However, the separation between transverse modes of a practical laser oscillator is of the order of megacycles and too small to be resolved spectroscopically.

There was reason to believe that the transverse modes would indeed be resolved. Theoretically, if an active medium is enclosed within the confines of a Fabry Perot interferometer, it can be shown that to a first approximation the output emission line width tends to zero when the gain perpass of the laser is greater than unity.¹⁰ Experimentally, oscillations had been observed both by time-resolved photography and electronic detection techniques. The oscillations in the megacycle range were tentatively explained, mainly by attributing them to beats between transverse modes - other explanations had, however, also been put forward.¹¹ It became the purpose of this project to study the oscillations in detail via experimental techniques, and attempt to arrive at the origin of the detected oscillations when sufficient data had been gathered. The results obtained seem to point inevitably to transverse modes as the origin of the oscillations. The results are in agreement with the predicted values of the difference frequencies.

Supporting evidence is provided by the mode patterns obtained by various workers who have photographed the face of active ruby lasers.

CHAPTER 2

RESONANT MODES IN A MASER INTERFEROMETER

2.1 Survey of the work of A. Fox and T. Li

We will consider the Integral Equation formulation of the problem relating to Transverse modes in a laser cavity.¹² The method is flexible in that it allows the representation of the mode structure for various geometries of the resonator. Although the problem can be formulated with little difficulty the solution requires using either the numerical approach coupled with the use of a high speed computer or, what is perhaps more desirable, the use of approximate analytic methods. Both approaches have been used and the results are available in the literature.¹³

If we consider an illuminated aperture, A , and we are given the aperture field, U_a , K being the propagation constant of the medium, we can write down the Fresnel field U_p at a point whose distance is R from the aperture, where R makes an angle θ with the unit normal to the aperture. U_p then is given by the surface integral,

$$U_p = \frac{jK}{4\pi} \int_A U_a \frac{e^{-jKR}}{R} (1 + \cos\theta) ds. \quad (1)$$

Use can be made of the Fresnel integral if it is assumed that given an optical cavity, a field distribution can be conceived to exist at one of the mirrors. This field distribution is in turn transferred to the opposite mirror via the surface integral transformation. The process is then repeated for the second mirror. This time the field distribution used is that caused originally by the first mirror on the second mirror.

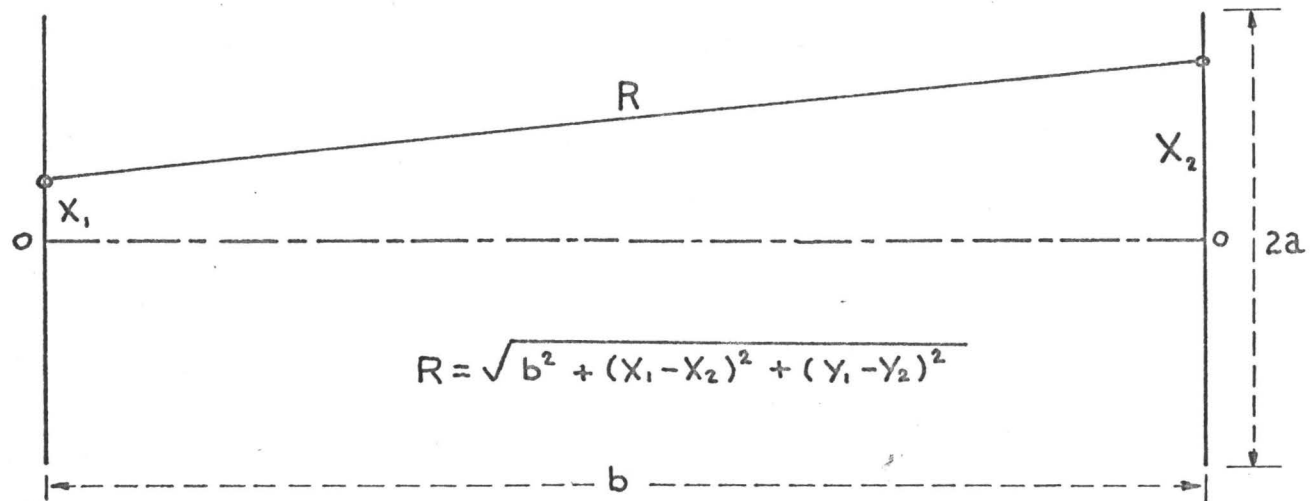
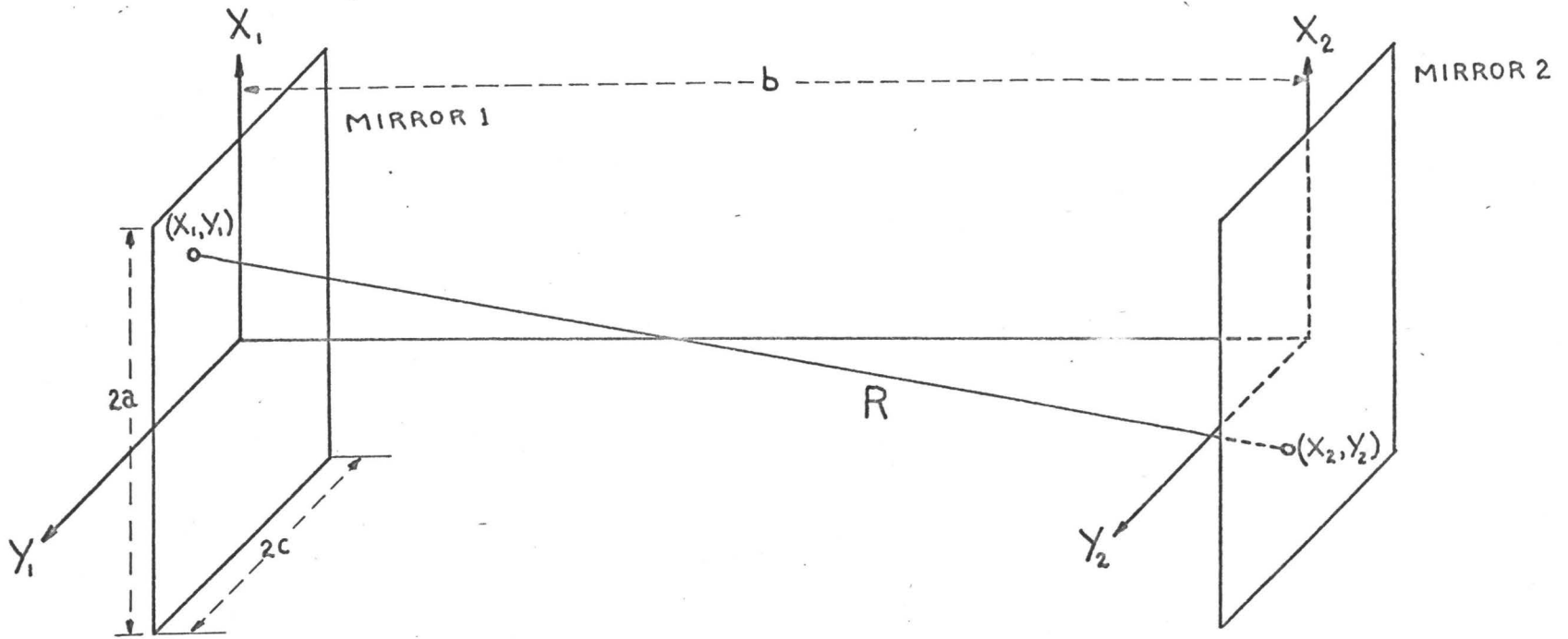


FIGURE 2.1 GEOMETRY FOR THE RECTANGULAR PLANE PARALLEL LASER CAVITY

Thus after q transits the field at a mirror due to the reflected field at the other is simply given by (1) with U_p replaced by U_{q+1} and U_a by U_q . Where U_q is the field after q transits and U_{q+1} is the field after $q+1$ transits.

There exists the possibility that after many transits the field may reach a steady state. Thus it is perhaps possible that,

$$\lim_{q \rightarrow \infty} U_{q+n} = C \lim_{q \rightarrow \infty} U_q$$

Thus a further n transits might leave the form of the field unchanged. The constant C would then take on in the general case a complex value. Its phase would measure the phase shift of the field after n transits and its magnitude the fractional field remaining after n transits.

Thus the phase shift per transit would be $\text{Arg } C^{1/n}$ and the amplitude loss per transit $(1 - |C^{1/n}|)$.

In particular, if we consider a single transit after the field has reached a steady state we can rewrite (1) as:

$$f = \frac{1}{C^{1/n}} \frac{jK}{4\pi} \int_A f \frac{e^{-jKR}}{R} (1 + \cos\theta) dS. \quad (2)$$

Where f is the steady state field distribution across either of the mirrors.

Explicitly we consider a rectangular cavity formed by two rectangular mirrors facing each other of dimensions a and c , separated by a distance b . Then $R = \sqrt{b^2 + (x_1 - x_2)^2 + (y_1 - y_2)^2}$

for $b/a \gg 1$, $b/c \gg 1$ (2) reduces to

$$f(x_2, y_2) = \frac{e^{-j\kappa b}}{c^{1/n}} \frac{j\kappa}{4\pi} \int_{-c}^c \int_{-a}^a f(x_1, y_1) e^{-\frac{j\kappa[(x_1-x_2)^2+(y_1-y_2)^2]}{2b}} dx_1 dy_1$$

valid only if $\frac{a^2}{b\lambda} \ll (b/a)^2$ and $\frac{c^2}{b\lambda} \ll (b/c)^2$

In the above, the approximation for R in the phase term of the exponential is a second order one, while only a first order approximation is used in the magnitude $\frac{1}{R}$. Thus we can write:

$$f(x_2, y_2) = \gamma \int_{-c}^c \int_{-a}^a K(x_1, x_2; y_1, y_2) f(x_1, y_1) dx_1 dy_1 \quad (3)$$

$$K(x_1, x_2; y_1, y_2) = \frac{j}{\lambda b} e^{-\frac{j\kappa[(x_1-x_2)^2+(y_1-y_2)^2]}{2b}}$$

$$\gamma = \frac{e^{-j\kappa b}}{c^{1/n}} \quad \kappa = \frac{2\pi}{\lambda} \quad \lambda \text{ is the wavelength in the medium.}$$

If $f(x_2, y_2) = v(x_2)g(y_2)$ it is possible to separate equation (3) into two equations each involving either x or y only:

$$v(x_2) = \gamma_x \int_{-a}^a K_x(x_2, x_1) v(x_1) dx_1 \quad (4)$$

$$g(y_2) = \gamma_y \int_{-c}^c K_y(y_2, y_1) g(y_1) dy_1 \quad (5)$$

$$K_x = \frac{e^{j\pi/4}}{\sqrt{\lambda b}} e^{-\frac{j\kappa(x_1-x_2)^2}{2b}}$$

$$K_y = \frac{e^{j\pi/4}}{\sqrt{\lambda b}} e^{-\frac{j\kappa(y_1-y_2)^2}{2b}}$$

$$\gamma_x \gamma_y = \gamma$$

(4) or (5) represents the integral equation for the infinite strip cavity with plane mirrors. This straightforward result can be arrived at from symmetry arguments, by assuming no variation in field along the infinite dimension of the strip. Thus a solution of the infinite strip problem will automatically solve the problem of the rectangular cavity with plane mirrors.

Equations (4) and (5) are homogeneous linear integral equations of the second kind. Since the kernel is continuous and symmetric $K(x_2, x_1) = K(x_1, x_2)$, and the eigen functions \mathcal{V}_n corresponding to distinct eigen values γ_n are orthogonal in the interval $(-a, a)$

$$\int_{-a}^a \mathcal{V}_n(x) \mathcal{V}_m(x) dx = 0 \quad m \neq n$$

The kernel is not Hermitian - a consequence of the inherently lossy system being considered. However, the eigen function of the non-Hermitian kernel can be expressed in terms of the eigen functions of an equivalent Hermitian kernel.

The eigen functions $\mathcal{V}_n(x)$ represent the possible normal distributions of the field across one of the mirror surfaces. They are the normal modes of the infinite strip cavity and are defined only on the mirror surface. They will in general be complex. Thus a real eigen function represents a mode that has constant phase across the mirror surface, while a complex eigen function represents a mode that has a phase variation across the mirror surface.

The eigen value γ_n is associated with the mode $\mathcal{V}_n(x)$ and will in general be complex. Its magnitude will be a measure of the loss per transit and its phase will be a measure of the phase shift per transit suffered by the particular mode $\mathcal{V}_n(x)$ as it propagates back and forth within the resonator.

In particular, $\log \gamma_n$ is the propagation constant of the mode represented by $\mathcal{V}_n(x)$. The real part of this constant specifies the loss per transit, while the imaginary part specifies the phase shift per transit that occurs in addition to the geometrical phase shift.

The problem stated in a straight forward manner is simply to find a set of functions $\mathcal{V}_n(x_1)$ such that when these are transformed via the integral equation (4) an identical functional variation $\mathcal{V}_n(x_2)$ will result.

Starting from the Fresnel integral we have shown that, once the condition of steady state is applied to the field distribution at the mirrors, an integral equation results. The solution of the integral equation gives the normal field distributions at the reflectors, as well as the losses and phase shifts associated with each normal mode.

The solution to the integral equation depends only on one parameter - namely the dimensionless constant $\frac{a^2}{b\lambda}$. The constant is referred to in the literature as the Fresnel number. Thus all resonators with the same Fresnel number will have identical field distributions when scaled down in the appropriate fashion. This result is true only in the case being considered - namely for $\frac{a^2}{b\lambda} \ll (b/a)^2$. For large values of $\frac{a^2}{b\lambda}$ the field for the lower order modes are weak at the edge of the resonator and the power loss per transit is, as a result, small for these modes.

Thus a wave launched initially will suffer almost negligible deterioration upon each passage for large values of $\frac{a^2}{b\lambda}$. Similarly the phase shift suffered by these low order modes will be small in the case of large values of $\frac{a^2}{b\lambda}$.

Computer solutions for the field distribution and in particular for the eigen values γ_n of the integral equation have been given by Fox and Li¹² for the range $20 > \frac{a^2}{b\lambda} > 0.5$. These solutions have been carried out, with reference to the appropriate integral equation, for circular plane mirrors, infinite strip mirrors and curved mirrors as well as for tilted plane mirrors. The method of solution employed yields only the first two lowest order modes.

The method of solution is numerical. The assumption is made that the modes representing the solution to the integral equation are characterized by a different loss per transit. The solutions of the integral equation are known to form a complete orthogonal set in the interval $(-a, a)$. Thus any excitation of the mirror can be represented by a sum in terms of this orthogonal set.

$$f(x) = \sum_{n=0}^{\infty} A_n v_n(x) \quad (6)$$

We transform (6) via the kernel and call the result $g_1(x)$

$$g_1(x_2) = \int_{-a}^a K(x_2, x_1) f(x_1) dx_1$$

We are given the orthogonal set characterizing the kernel $K(x_2, x_1)$

$$\text{i.e. } v_n(x_2) = \lambda_n \int_{-a}^a K(x_2, x_1) v_n(x_1) dx_1$$

Thus after one transit $f(x)$ is transformed into $g_1(x) = \sum_{n=0}^{\infty} A_n \gamma_n v_n(x)$.

After q transits $f(x)$ is transformed into $g_q(x)$

$$g_q(x) = \sum_{n=0}^{\infty} A_n \gamma_n^q v_n(x).$$

The eigen values are assumed to be numbered in such a way that

$$|\gamma_0| > |\gamma_1| > |\gamma_2| \dots \dots \dots |\gamma_n| > |\gamma_{n+1}| \dots \dots$$

The weight or coefficient of $v_n(x)$ after q transits is thus

$A_n (\gamma_n)^q$. Initially the relative weights of the coefficients with respect to the coefficient of the lowest order eigen function were

$\frac{A_n}{A_0}$ this ratio has now become $\frac{A_n (\gamma_n)^q}{A_0 (\gamma_0)^q}$ after q transits. In particular $\lim_{q \rightarrow \infty} \frac{A_n (\gamma_n)^q}{A_0 (\gamma_0)^q} \rightarrow 0 \quad n \neq 0$

Thus the initially launched wave has been distorted in such a manner as to contain mainly the lowest order mode, after it has undergone a sufficient number of transits. The lowest order mode can therefore be solved for by simply iterating any initial distribution except a field distribution where $A_0 = 0$. In practice the lowest order even mode and the lowest order odd mode can be solved for, by launching an excitation that is either even or odd respectively. This is a consequence of the symmetry of the kernel. The kernel considered has either even or odd solutions. Even and odd modes do not mix.

We have discussed some of the properties of the integral equation connected with plane parallel rectangular resonators and have indicated

a possible method of solution. The general properties so discussed are applicable to those other commonly used resonator geometries.

We will undertake in the next section to develop the integral equation for cylindrical cavities and discuss a powerful method of obtaining its solution.

2.2 Solution of the Integral Equation for Circular Plane Mirrors

Consider two circular plane mirrors forming an optical resonant cavity. The Fresnel field of the first mirror on the second after q transits may be written as $U_{q+1}(r_2, \phi_2)$. The field on the first mirror is $U_q(r_1, \phi_1)$. Under cylindrical symmetry the integral equation is written:

$$U_{q+1}(r_2, \phi_2) = \frac{j}{2\lambda} \int_0^a \int_0^{2\pi} U_q(r_1, \phi_1) e^{-j\frac{\kappa R}{R}} \left(1 + \frac{b}{R}\right) r_1 d\phi_1 dr_1$$

where $R = \sqrt{b^2 + r_1^2 + r_2^2 - 2r_1 r_2 \cos(\phi_1 - \phi_2)}$

for b/a large we can write:

$$U_{q+1}(r_2, \phi_2) = \frac{e^{j\kappa b}}{\lambda b} \int_0^a \int_0^{2\pi} U_q(r_1, \phi_1) e^{-j\kappa \left[\frac{r_1^2 + r_2^2}{2b} - \frac{r_1 r_2}{b} \cos(\phi_1 - \phi_2) \right]} r_1 d\phi_1 dr_1$$

valid for $\frac{a^2}{b\lambda} \ll (b/a)^2$.

The integral equation becomes

$$v(r_2, \phi_2) = \gamma \int_0^a \int_0^{2\pi} K(r_2, \phi_2; r_1, \phi_1) v(r_1, \phi_1) r_1 d\phi_1 dr_1 \quad (7)$$

$$K(r_2, \phi_2; r_1, \phi_1) = \frac{j}{\lambda b} e^{-j\kappa \left[\frac{r_1^2 + r_2^2}{2b} - \frac{r_1 r_2}{b} \cos(\phi_1 - \phi_2) \right]}$$

with $e^{-jk b}$ being absorbed in γ .

It is known that:

$$e^{jn[\frac{\pi}{2} - \phi_2]} J_n\left(\kappa \frac{r_1 r_2}{b}\right) = \frac{1}{2\pi} \int_0^{2\pi} e^{jk \frac{r_1 r_2}{b} \cos(\phi_1 - \phi_2) - jn\phi_1} d\phi_1 \quad (8)$$

integrating (7) after making use of (8) it is seen that

$$v(r, \phi) = R_n(r) e^{-jn\phi} \quad n = \text{integer}$$

satisfies (7).

Then $R_n(r)$ satisfies

$$R_n(r_2) \sqrt{r_2} = \gamma_n \int_0^a K_n(r_2, r_1) R_n(r_1) \sqrt{r_1} dr_1 \quad (9)$$

with

$$K_n(r_2, r_1) = \frac{j^{n+1} \kappa}{b} J_n\left(\kappa \frac{r_1 r_2}{b}\right) \sqrt{r_1 r_2} e^{-j\kappa \frac{(r_1^2 + r_2^2)}{2b}}$$

where J_n is a Bessel function of the first kind and n th order.

$$\text{Let } \rho = r/a \text{ and } H = \frac{2a^2}{b\lambda}$$

Then (9) becomes:

$$R_m(\rho) = \gamma_m j^{m+1} \pi H \int_0^1 R_m(\rho_1) J_m(\pi H \rho \rho_1) e^{-j\frac{\pi}{2} H(\rho^2 + \rho_1^2)} \rho_1 d\rho_1 \quad (10)$$

It is important to note that the solution of (10) depends only on the

single parameter H . The parameter H is, of course, the Fresnel number.

Fox and Li use $N = \frac{a^2}{b\lambda}$ as the Fresnel number. In this treatment, however,

H is the Fresnel number with $H = 2N$.

It is known that for large values of H the field distribution over the reflector surface approaches the distribution of the modes of a circular waveguide with conducting walls, since for such large values of

If the losses will be small as will be the magnitude of the field at the mirror perimeter. Thus boundary conditions similar to those employed in circular waveguide theory apply. We thus write following Bergstein & Schachter¹³

$$R_m(\rho) = \sum_{k=1}^{\infty} C_{mk} \frac{\sqrt{2}}{J'_m(P_{mk})} J_m(P_{mk}\rho) \quad (11)$$

where J_m is the Bessel function of the first kind of order m and J'_m its first derivative. P_{mk} is the k th zero of the Bessel function J_m .

$$J_m(P_{mk}) = 0 \quad K = 1, 2, 3 \dots$$

substituting (5) into (4) we write:

$$\frac{1}{\gamma_m} \sum_{k=1}^{\infty} \frac{C_{mk} \sqrt{2}}{J'_m(P_{mk})} J_m(P_{mk}\rho) = \int_0^1 \frac{m+1}{\pi H} e^{-\frac{j}{2} \pi H(\rho^2 + \rho_1^2)} J_m(\pi H \rho, \rho) \left[\sum_{k=1}^{\infty} \frac{C_{mk} \sqrt{2}}{J'_m(P_{mk})} J_m(P_{mk}\rho_1) \right] \rho_1 d\rho_1 \quad (12)$$

Recalling that $\int_0^1 J_m(P_{mk}\rho) J_m(P_{mn}\rho) \rho d\rho = 0 \quad n \neq k$

and $\int_0^1 J_m^2(P_{mk}\rho) \rho d\rho = \frac{[J'_m(P_{mk})]^2}{2}$

and multiplying both sides of (12) by ρ times the complex conjugate of the left hand side and integrating over ρ from 0 to 1 we get:

$$\frac{1}{\gamma_m} \sum_{j=1}^{\infty} |C_{mj}|^2 = \sum_{j,k} (A_{m,jk} C_{m,j}^* C_{mk})$$

Where

$$A_{m,jk} = e^{-j(m+1)\frac{\pi}{2}} \left[\frac{2\pi H}{J'_m(\rho_{mk})J'_m(\rho_{mj})} \right] \int_0^1 \int_0^1 e^{j\frac{\pi}{2}H(\rho_i^2 + \rho^2)} J_m(\pi H \rho \rho_i) J_m(\rho_{mk} \rho) J_m(\rho_{mj} \rho_i) \rho \rho_i d\rho d\rho_i$$

From Ritz's variational method we know that the eigen values γ_{mn} are determined from the condition

$$\sum_{k=1}^{\infty} (A_{m,jk} - \frac{1}{\gamma_m} \delta_{j,k}) C_{mk} = 0 \quad \text{for every } j$$

This represents an infinite system of homogeneous linear simultaneous equations in the unknown coefficients C_{mk} . It admits non-zero solutions only if the determinant of the coefficients vanishes, i.e.

$$\left[A_{m,jk} - \frac{1}{\gamma_m} \delta_{j,k} \right] = 0$$

The roots of this equation are the eigen values $\frac{1}{\gamma_{mn}}$ of the integral equation.

The elements $A_{m,jk}$ must be evaluated to proceed further. We write

$$\int_0^1 \int_0^1 f(\rho, \rho_i) d\rho d\rho_i = I(0,0) - I(0,1) - I(1,0) + I(1,1)$$

Where

$$I(b,c) = \int_{\rho=b}^{\infty} \int_{\rho_i=c}^{\infty} f(\rho, \rho_i) d\rho d\rho_i$$

The integrals $I(0,0)$, $I(0,1)$ and $I(1,0)$ can be readily evaluated. The integral $I(1,1)$ is evaluated by replacing the Bessel functions by their asymptotic expansion. That is to say $J_m(\alpha) \approx \left(\frac{2}{\pi\alpha}\right)^{1/2} \cos\left(\alpha - \frac{\pi}{4} - m\frac{\pi}{2}\right)$

When these integrals are evaluated it is found that for $H > 5$ say, the

off-diagonal elements are small compared with the diagonal elements.

Thus

$$|A_{m,jk}| \ll |A_{m,kk}| \quad H \gg 5$$

This gives:

$$\frac{1}{\gamma_{mn}} \approx A_{m,nn}$$

and

$$f_{mn}(\rho, \phi) = e^{-j m \phi} R_{mn}(\rho) \doteq [\pi^{1/2} J'_m(P_{mn})]^{-1} J_m(P_{mn} \rho) e^{-j m \phi}$$

solving for γ_{mn} gives:

$$\gamma_{mn} \doteq \left(1 + \frac{(P_{mn}/\pi)^2}{3 H H^{1/2}} \right) e^{-\frac{i\pi (P_{mn}/\pi)^2}{2 H}} \quad \text{for } H > (P_{mn}/\pi)^2$$

2.3 Equation for the Beats Between Transverse Modes

The eigen value of the integral equation relevant to cylindrical geometry has been shown to be

$$\gamma_{mn} \doteq \left(1 + \frac{(P_{mn}/\pi)^2}{3 H H^{1/2}} \right) e^{-\frac{i\pi (P_{mn}/\pi)^2}{H}}$$

by Bergstein and Schachter¹³ for

$$H > (P_{mn}/\pi)^2$$

The propagation constant in the resonator is thus K_R

$$K_R = \log_e [\gamma_{mn} e^{-iKb}]$$

$$= \log_e \left[1 + \frac{(P_{mn}/\pi)^2}{3HH^{1/2}} \right] - iKb - \frac{i\pi (P_{mn}/\pi)^2}{2H}$$

The imaginary component $Kb + \frac{\pi (P_{mn}/\pi)^2}{2H}$ specifies the wavelength of the electromagnetic energy within the cavity. The real part specifies the losses. The oscillating frequency is thus f_{mn} where

$$f_{mn} = \frac{c}{\mu\lambda_0} + \frac{c P_{mn}^2}{b4H\pi^2\mu} = \frac{c}{\mu\lambda_0} + \frac{\lambda_0 c P_{mn}^2}{\mu^2 8\pi^2 a^2}$$

The beat frequency is thus given by Δf

$$\Delta f = (f_{mn} - f_{m'n'}) = \frac{\lambda_0 c}{\mu^2 8\pi^2 a^2} (P_{mn}^2 - P_{m'n'}^2)$$

where λ_0 - is the free space wavelength

c - is the speed of light in vacuum

a - is the resonator radius

μ - is the index of refraction of the active medium

and $J_m(P_{mn}) = 0$.

CHAPTER 3

EVIDENCE FOR EXISTENCE OF TRANSVERSE MODES

3.1 Brief Survey of Stickley's Work

Stickley⁷ was the first to recognize the possibility of observing transverse mode beat frequencies based on the results of high speed photographs of the near field radiation patterns of ruby. It had been observed that different transverse mode patterns could indeed occur simultaneously in an active resonator. The iterative calculations of Fox and Li¹² showed that transverse modes were natural solutions to the integral equation describing the fields in the resonator. These transverse modes by virtue of their different spatial distributions suffered a phase shift (leading relative to the geometrical phase shift) that was different for each mode. The numerical calculations of Fox and Li for the beat frequencies showed that for $\frac{a^2}{b\lambda} \gg 10$ the beat frequencies could be calculated from the formula:

$$\Delta f = \frac{\lambda_0 c}{\mu^2 8\pi^2 a^2} [P_{mn}^2 - P_{m'n'}^2] \quad J_m(P_{mn}) = 0$$

Stickley made use of this evidence, in an attempt to detect the beat frequencies by use of the square law response of a photomultiplier. He successfully detected the beat frequencies but did not test the validity of the equation describing them.

In later experiments by Stickley, where the output of a ruby laser was monitored by a fast camera as well as by a photomultiplier, negative results were obtained.¹⁴ The beat frequencies could not be correlated with the observed patterns on the ruby face.

It is felt that a tentative explanation of Stickley's negative results rests on the fact that the beat frequencies in a given spike are generally small compared to the total light output in the spike, and so photographic techniques would appear not to be able to detect two modes with say a factor of ten or even a hundred between their relative intensities.

It has been found experimentally that beat frequencies are observed much more often at 77°K than at room temperature. Operation at low temperatures (77°K) also seems to result in stronger beats; the beats being clearly visible on the relaxation spike when the light is detected with a fast detector and the output from the detector monitored on an oscilloscope. As expected, the observed beats at 200°K were weaker than those observed when a crystal temperature of 77°K was employed. Since 200°K is the temperature at which Stickley performed his runs, it is likely that the modes from which he detected the beat frequencies were combinations of either moderately weak modes or strong and weak modes. This would, of course, result in weak beat frequencies. The terms "strong" and "weak" are used with reference to the total light output in the spike. Thus, in view of the only moderately low temperatures used by Stickley it is not surprising that his photographic techniques did not correlate to his electronic techniques for observing the beat frequencies.

3.2 Modes in Dielectric Optical Waveguides

Some good work has been carried out by Snitzer on optical dielectric waveguides.¹⁵ He has presented the solution of Maxwell's equations in cylindrical geometry for the system composed of a high index of refraction core and a low index of refraction cladding. Four sets of modes are found to exist, namely the transverse electric (TE_{0m}), the transverse magnetic (TM_{0m}), and the hybrid modes EH_{nm} and HE_{nm}. He has carried out experimental work on the systems described in his analysis, using cylinders with core diameters in the order of 25μ. By illuminating one end of the fibre and observing the other end, he had obtained some very striking photographs of the modes of propagation in clad fibres.

By considering the Fabry-Perot interferometer as a dielectric waveguide he has derived the equation for the frequency separation between transverse modes. This is the same equation arrived at from other considerations as outlined previously, namely

$$\Delta f = \frac{c \lambda_0}{8\pi^2 a^2 \mu^2} [P_{nm}^2 - P_{n'm'}^2]$$

The conditions used by Snitzer to arrive at this result are that the waveguide is operating far from cut-off, and that the index of refraction difference between core and cladding tends to zero. These conditions are just the conditions encountered in the clad ruby used in our experiments.

Consider a dielectric core of index of refraction n_1 , free space magnetic permeability μ and radius a . The core is assumed to be imbedded in a dielectric medium of lower index of refraction n_2 .

Cylindrical coordinates are chosen. Conventionally we call these coordinates r, θ, z . Then the field components in the core can be written as:

$$E_r = \frac{iha}{u} \left[\frac{i-P}{2} J_{n-1} - \frac{1+P}{2} J_{n+1} \right] F_c$$

$$E_\theta = \frac{iha}{u} \left[-\frac{1-P}{2} J_{n-1} - \frac{1+P}{2} J_{n+1} \right] F_s$$

$$H_r = -\frac{iK_1^2 a}{\mu\omega u} \left[-\frac{1-P h^2/K_1^2}{2} J_{n-1} - \frac{1+P h^2/K_1^2}{2} J_{n+1} \right] F_s$$

$$H_\theta = \frac{iK_1^2 a}{\mu\omega u} \left[\frac{i - P h^2/K_1^2}{2} J_{n-1} - \frac{1+P h^2/K_1^2}{2} J_{n+1} \right] F_c$$

$$E_z = J_n(ur/a) F_c$$

$$H_z = -\frac{h}{\mu\omega} P J_n(ur/a) F_s$$

where

$$F_c = A \cos(n\theta + \psi_n) e^{i(hz - \omega t)}$$

$$F_s = A \sin(n\theta + \psi_n) e^{i(hz - \omega t)}$$

$$K_1 = 2\pi n_1/\lambda$$

The field in the cladding (i.e. the medium in which the core is imbedded) of index of refraction n_2 is given by equations similar to those above, but with the propagation constant K_1 replaced by K_2 and the radial dependence in terms of the Bessel functions J_n replaced by modified Hankel functions. The latter functions tend monotonically to zero as $r \rightarrow \infty$. The phase ψ_n can take on values 0 and $\pi/2$. The relation between the parameters u and h is

$$(u/a)^2 = K_1^2 - h^2$$

Their values and P are found from the boundary conditions.

A mode is specified by two subscripts and a letter designation. The subscripts are n and m , the latter being the successive root of the Bessel function J_n that u is near. The cylindrically symmetric ($n = 0$) modes are transverse electric (TE $_{0m}$) or transverse magnetic (TM $_{0m}$) as in the metallic waveguide. However, the higher-order modes are hybrid, i.e. they have non-vanishing values for both F_z and H_z . They are designated EH $_{nm}$ and HE $_{nm}$. They result from the two possible values which P can assume for fixed n and m .

We are interested in the solution of the above equations for the condition far from cut-off and vanishingly small indices of refraction between core and cladding. The conditions outlined are just the conditions applicable to the ruby laser which we studied experimentally.

Under far from cut-off conditions the values of u are solutions of,

$$J_{n+1}(u) = 0 \text{ for the TE}_{0m}, \text{ TM}_{0m} \text{ and EH}_{nm} \text{ modes.}$$

On the other hand, considering the HE $_{nm}$ modes the values of u are found from the equation:

$$J_{n-1}(u) = 0.$$

For $n_1 - n_2$ small the guide propagation constant h approaches K_1 and the parameter P is equal to $+1$ for the EH modes and -1 for the HE modes. Thus from the equations for the field components we see that the radial dependence of the transverse components of the field is in terms of J_{n+1} for the EH $_{nm}$ modes and J_{n-1} for the HE $_{nm}$ modes.

From the integral representation of the Bessel functions, a waveguide mode can be considered as a properly phased array of interfering plane waves, all of whose wave normals make the same angle ϕ with the guide axis. From an effective index of refraction n_e and a guide wavelength γ_g can be defined by

$$h = 2\pi/\lambda_g = 2\pi n_e/\lambda$$

and $n_e = n_1 \cos \phi$.

Then, using $(u/a)^2 = k_1^2 - h^2$

we arrive at $\sin \phi = \frac{u}{2\pi n_1} \frac{\lambda}{a}$

For far from cut-off conditions $\sin \phi \approx \phi$

therefore $\phi \approx \frac{u \lambda}{2\pi n_1 a}$

The resonance condition for two modes 1 and 2 can be written as:

$$L = \frac{N\lambda}{2n_1 \cos \phi}$$

or

$$\frac{NC}{2Ln_1} = f_1 \cos \phi_1 = f_2 \cos \phi_2$$

Where f_1 and f_2 are the frequencies of the two modes being considered.

Therefore

$$\begin{aligned} \Delta f = f_1 - f_2 &= \frac{NC}{2Ln_1 \cos \phi_1} - \frac{NC}{2Ln_1 \cos \phi_2} \\ &= \frac{NC}{2Ln_1} \left[1 + \frac{\phi_1^2}{2} - 1 - \frac{\phi_2^2}{2} \right] \\ &= \frac{NC}{4Ln_1} [\phi_1^2 - \phi_2^2] \\ &= \frac{\lambda C}{8\pi^2 a^2 n_1^2} [u_1^2 - u_2^2] \end{aligned}$$

This formula is seen to be identical to that arrived at from the solution to the integral equation. The equation is further verified by the numerical calculations of Fox & Li for conditions far from cut-off (i.e. the low loss region).

CHAPTER 4

DESCRIPTION OF APPARATUS

4.1 Laser Head and Power Supply

The laser head used in the experiments to measure beat frequencies was of the elliptic type. The crystal is supported along one focus of the ellipse with the flashtube positioned along the other focus. Thus, considering the case of ideal geometry, light emanating from a line source on one focus will be focused as a line image on the other focus. It is seen, therefore, that light from the flashtube will be concentrated on the crystal as long as the flashtube and crystal diameters are small compared to the dimensions of the ellipse. In our case the ellipse dimensions were

major axis 5"

minor axis $4\frac{1}{2}$ "

distance between foci $2\frac{1}{8}$ "

The crystal diameter including the cladding was $1/5$ " and the flashtube diameter $1/4$ ".

The elliptical reflectors were of polished aluminum. They were found to be durable and easily cleaned. Their high polish has not deteriorated appreciably in a year.

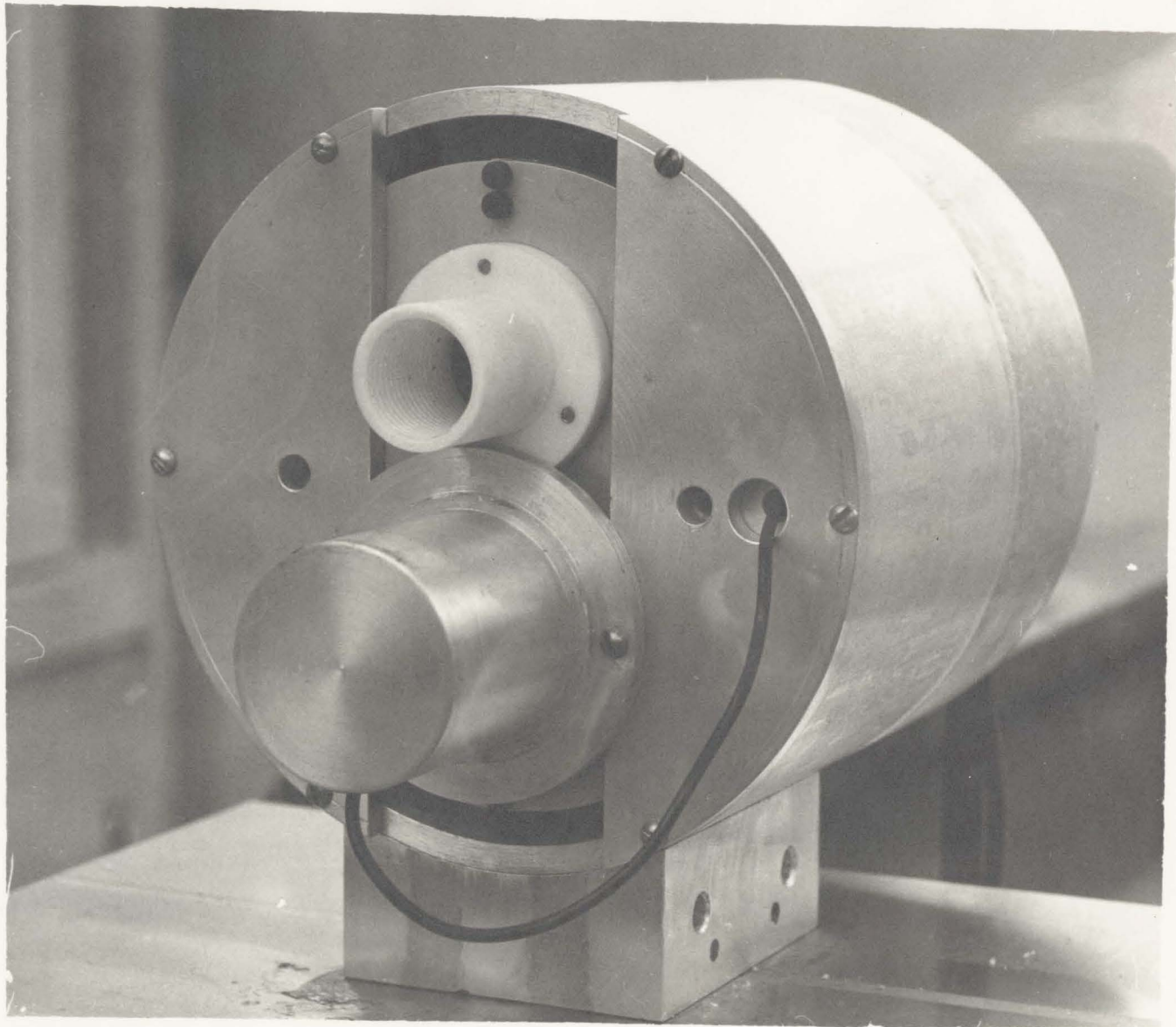
Cooling of the flashtube could be accomplished either by high velocity air for room temperature operation, or by the low temperature nitrogen atmosphere employed when cooling the ruby crystal by conduction

to 77°K. The nitrogen atmosphere was provided by feeding the laser head with nitrogen gas evaporated from a liquid nitrogen dewar. Since the ruby crystal was cooled to liquid nitrogen temperatures, it was found necessary to provide a dry atmosphere within the laser head to prevent frosting of the entire system. The ruby was held in an aluminum holder which was equipped with a tank well insulated from its surroundings. The tank could be filled with liquid nitrogen. Heat from the ruby was conducted away through the holder to the liquid nitrogen bath.

The ruby was also surrounded by the cool stream of nitrogen gas, minimizing the rate of heat flow to the nitrogen tank necessary to keep the ruby at liquid nitrogen temperatures, thus lowering the temperature gradient between bath and crystal. The resistance of the holder to heat flow was kept low by allowing the heat transfer to take place between the crystal and bath through as much bulk aluminum as practically possible. Heat was mainly conducted to the nitrogen bath through an area of 4 square inches. The temperature gradient between bath and crystal was thus not more than 10°C.

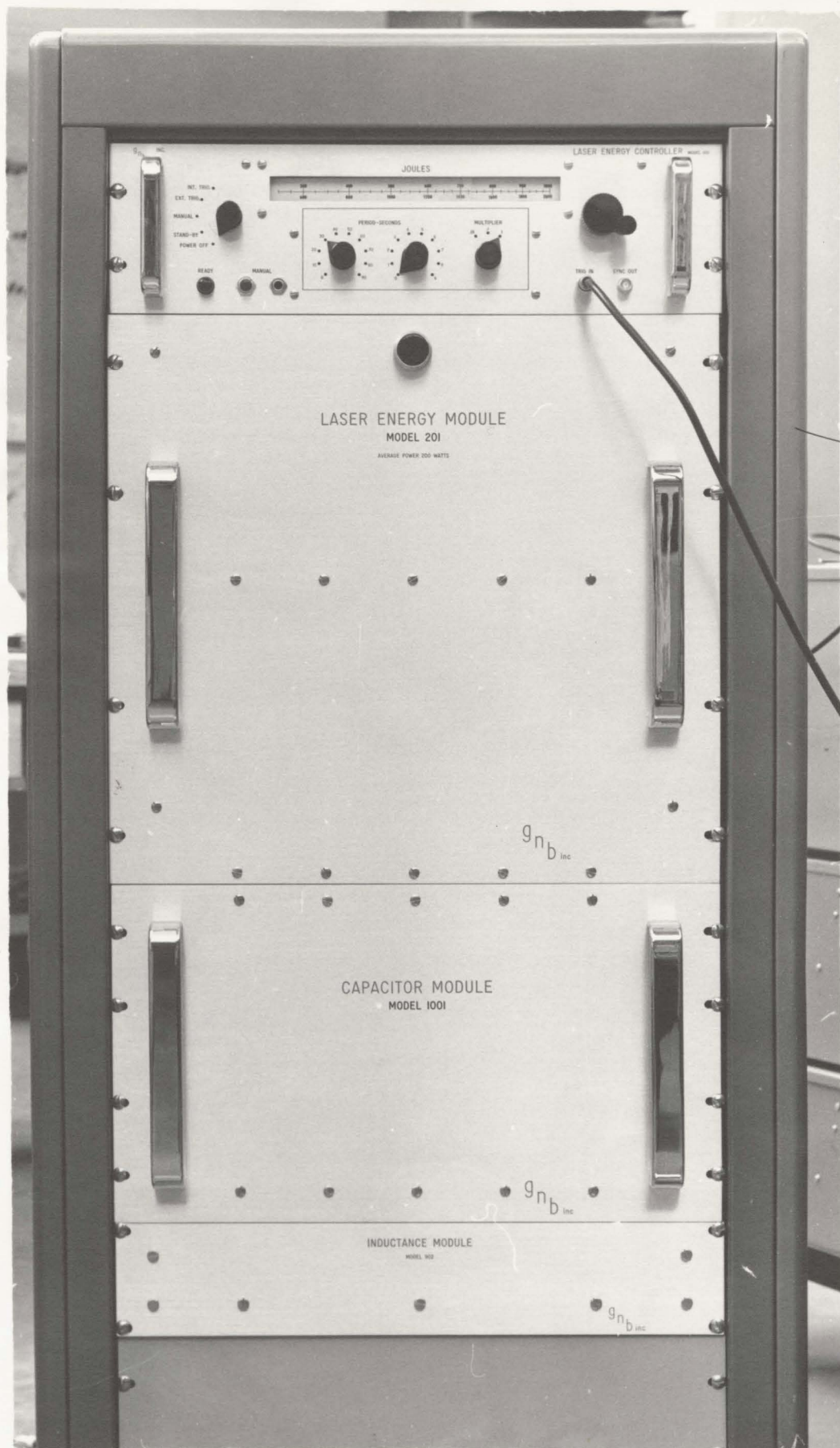
The power supply used to trigger and energize the flashtube was a GNB model 20-002. The unit is composed of 8 capacitor banks each capable of storing 250 joules of energy at 2200 volts, the maximum rated voltage of the supply. The minimum output energy obtainable is 62.5 joules at 1000 volts. The capacitor banks are easily connected in parallel to cover the range 2000 to 62.5 joules of output energy.

The supply energy is controlled by the Controller Module. The flashtube supports easily a potential difference of 2200 volts across its



THE ELLIPTICAL LASER HEAD

FIGURE 4.1



THE LASER POWER SUPPLY

FIGURE 4.2

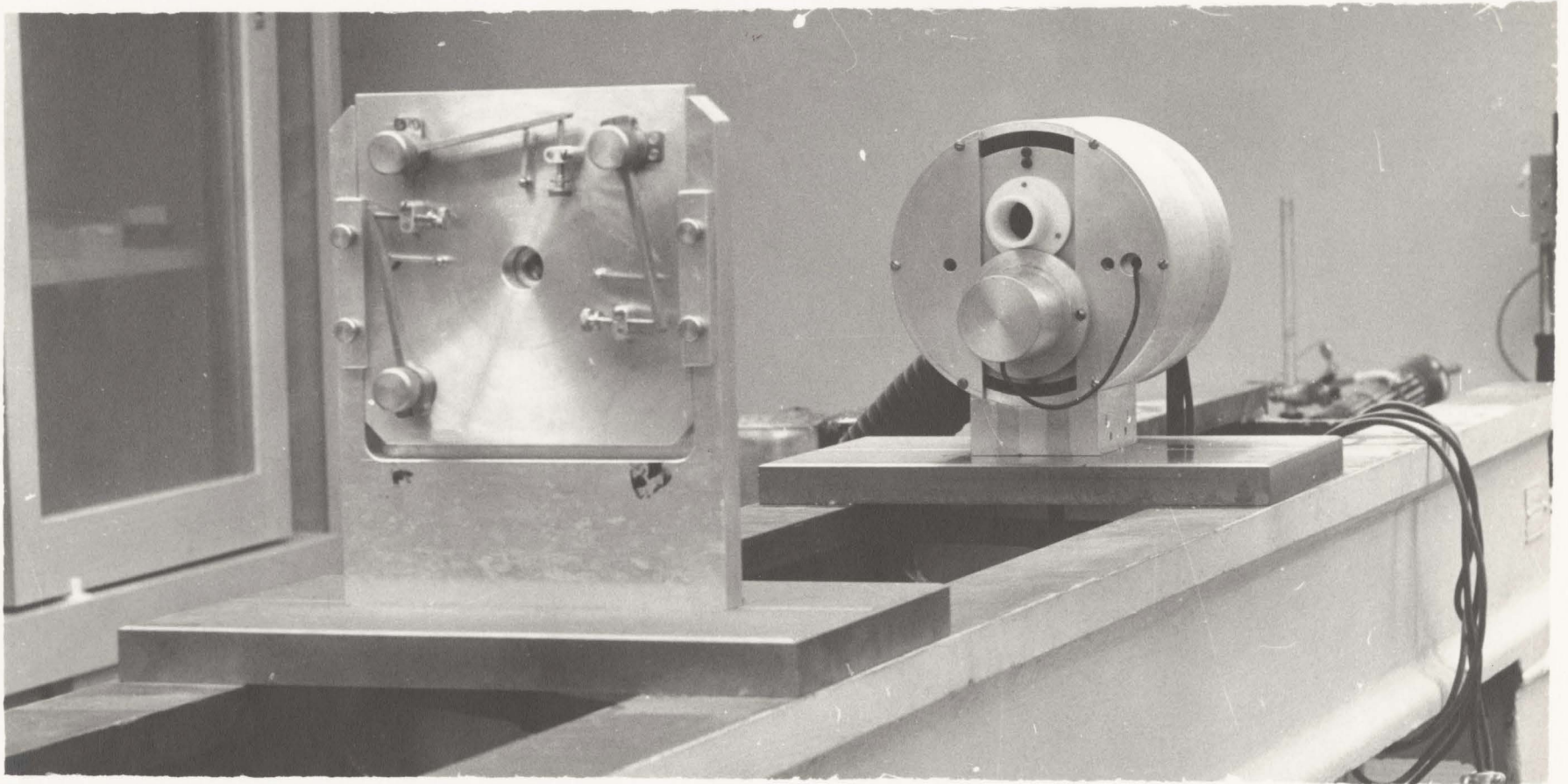
terminals until a 20,000 volt trigger is supplied to a coarse ($\frac{1}{2}$ inch) grid surrounding the flashtube. The trigger breaks down the Xenon in the flashtube allowing the electrical energy previously being held back by the unionized Xenon to be converted into useful light output and heat.

The controller module controls the trigger, which can be activated in three ways

- 1) manually
- 2) automatically with a period ranging from 0.01 seconds to 100 seconds
- 3) by an external +10 volt pulse into 4000 ohms.

The average output power may not exceed the linear charging rate of 200 joules per second. The pulse from the thyatron that generates the flashtube trigger pulse is used to generate a +2 volt pulse from 100 ohms used for external synchronizing purposes.

The Energy Module is used to generate a linear charging rate of 200 joules/second, until a predetermined voltage is reached. The voltage is controlled from the panel of the controller module. A pointer on the controller module reads output energy directly in joules. Scales are interchangeable for different capacitor bank connections. An inductance module is provided consisting of two 800 millihenry coils each tapped at 100, 200, and 400 millihenries. This permits interconnections to be made between the chokes and the capacitor banks for use as current limiting chokes or to simulate the discharge from a transmission line and so approach a rectangular shaped light output pulse from the flashtube.



THE LASER HEAD AND EXTERNAL MIRROR HOLDER MOUNTED ON THE LATHEBED

FIGURE 4.3

4.2 Mounting

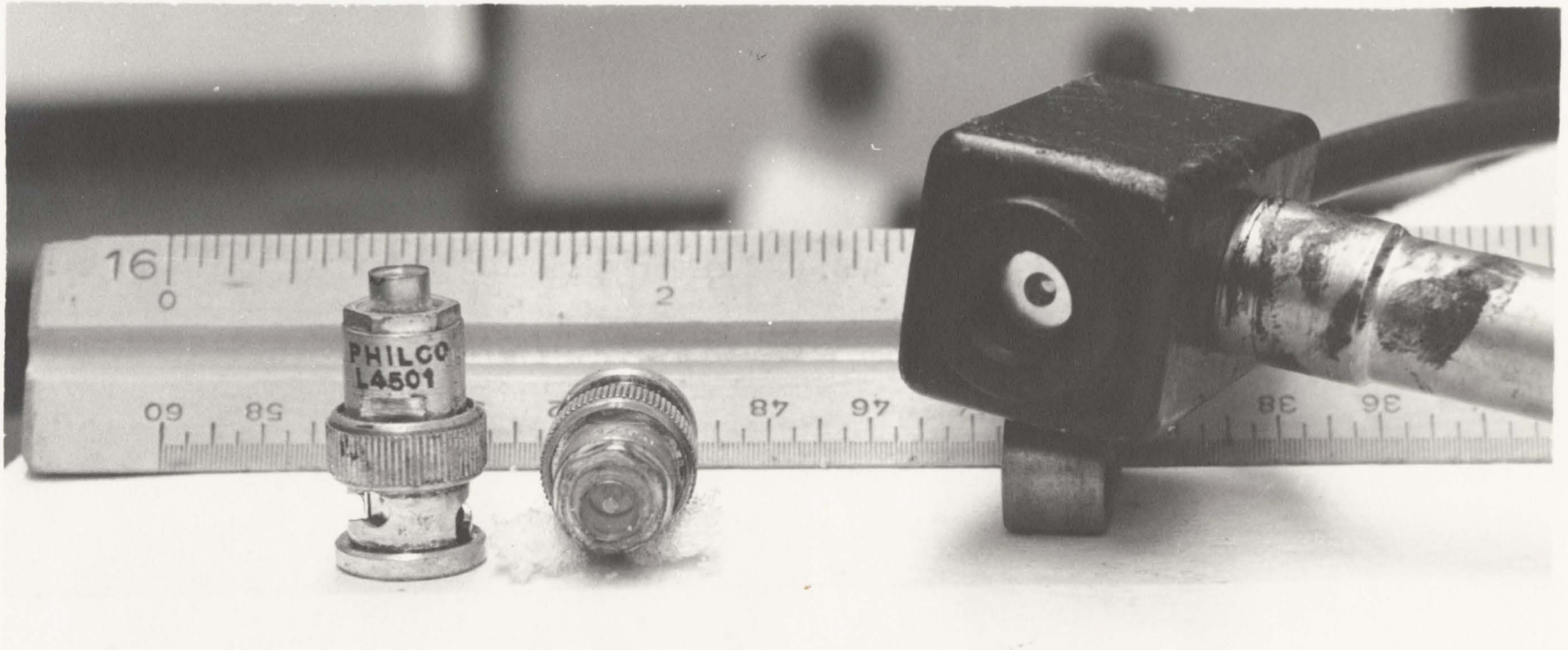
The elliptical laser head was mounted on a $\frac{1}{2}$ " steel plate which was bolted rigidly to an eight foot lathe bed. The laser head could be placed at will on any required location along the lathe bed guides.

An external mirror mount was designed and built. It was mounted on a $\frac{1}{2}$ " steel plate to give rigidity and freedom from vibration. Autocollimation experiments on the mirror holder showed that it could be easily and rapidly adjusted to a relative parallelism of 0.5 seconds of arc. Settings could be made anywhere within a 10° range. The system was stable and a sharp reflected crosshairs was obtained on autocollimation, showing that spurious vibration was not greater than 0.1 seconds of arc, the resolution of the autocollimator used.

The system is thus versatile and can be easily converted into a Q-spoiling device with little, if any, modifications.

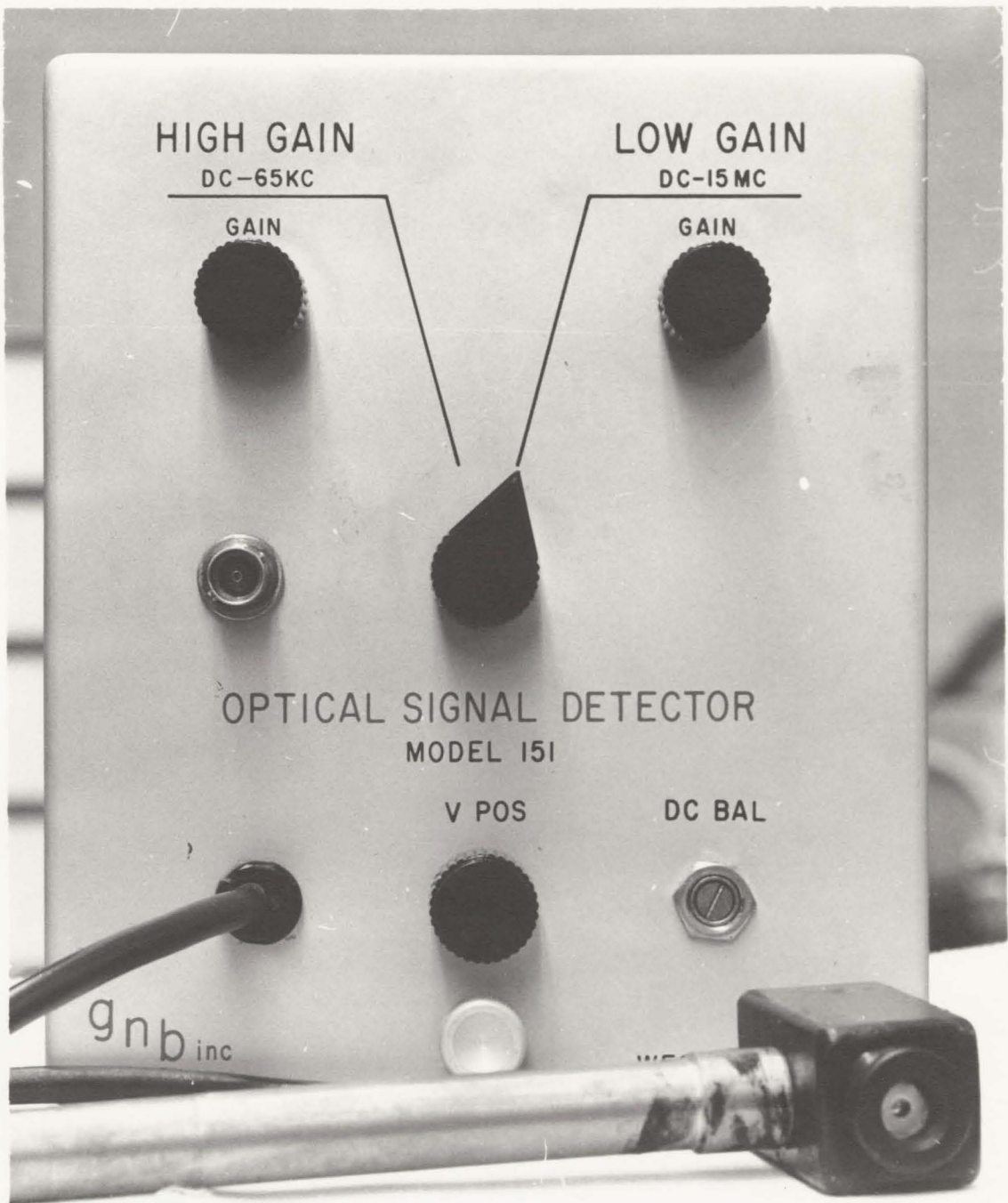
4.3 Detectors

The detection of beat signals depends primarily on the non-linearity of the detecting device. The detecting devices available are mainly square law in the range of operation. They are the standard phototube, the photomultiplier, and the backbiased diode junction. A prerequisite of these devices is that they be fast enough to follow the variations in the signal being detected. The phototube and the photomultiplier are fast enough to be useful in the range 0-60 Mg., when the circuitry is appropriately designed. Experimentally, a 100 ohm load gave the required response. A short calculation shows that this is not unreasonable. The high frequency response is governed by the shunt capacitance across the detector.



TWO TYPES OF DIODE OPTICAL DETECTORS CAPABLE OF A FAST RESPONSE TIME

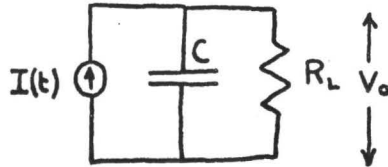
FIGURE 4.4



AN OPTICAL SIGNAL DETECTOR UNIT

FIGURE 4.5

We can represent the detector by a current source in parallel with the stray capacitance feeding a load resistor R.



In general $I(t)$ will not be a sinusoidally varying signal. However, we can simply consider it to be representative of one of the Fourier components of the net current $I(t) = \sum_{n=0}^{\infty} A_n I_n(\omega_n t)$. Then the associated Fourier component of the output voltage is

$$V_o(\omega_n t) = I_n(\omega_n t) \left(\frac{1}{R_L} + j\omega_n C \right)^{-1}$$

$$|V_o(\omega_n t)| \text{ will go to } \frac{|I(\omega_n t)| R_L}{\sqrt{2}} \text{ at } \omega_n = \frac{1}{RC}$$

$$\text{or at } f_n = \frac{1}{2\pi RC}$$

with $f = 60 \text{ Mc}$ and $R = 100 \Omega$

we can solve for C. $C = 26.5 \times 10^{-12}$ farads.

The value of C is seen to be typical of the order of magnitude of strays. Loading a photomultiplier with a cathode follower with an input impedance of 500Ω has resulted in an increased gain (5X) without appreciably spoiling the frequency response of the photomultiplier. Thus stray capacity was essentially reduced to 5 p.f. and was hence shown to be the dominating capacitance in the circuit.

Since the experiments carried out in this project were undertaken mainly with the use of a back-biased diode it is perhaps useful to consider the theory of such a device.^{16,17} The back-biased diode is an efficient

detector of quanta whose wavelengths are shorter than the fundamental absorption edge. This is because each photon absorbed creates a hole-electron pair.* The pair will drift and if it reaches the junction it will be split up by the reverse-bias field. The hole will be collected in the P region and the electron in the N region of the device. State of the art photodiode detectors have a quantum efficiency approaching unity. This means that almost one unit of charge flows through the circuit for each incident photon.

Consider a planar junction of area A with light incident normal to the surface of the junction. A DC voltage source V is connected in series with a load resistance R and the diode detector in such a way that it reverse biases the diode junction. A depletion region of thickness Y will be created at the junction separating the N type semiconductor from the P type. The Fermi levels will be appropriately displaced in energy by V electron volts, the level of the P type lying above the level of the N type.

Suppose there are F photons per second incident on the diode. The current I_0 that will flow in the circuit will be given by

$$I_0 = q\alpha F$$

where q is the fundamental electron charge

α is the quantum efficiency

F is the number of photons per second.

The quantum efficiency, as has been mentioned previously, is a measure of the number of hole electron pairs created by a single incident photon. It is generally of the order of unity for state of the art diode detectors, however it is not difficult to imagine a situation where charge multiplication would occur. Consider a junction back biased with a voltage V , an electron traversing the depletion region would convert its potential energy V electron volts into kinetic energy V electron volts as it fell through the biasing potential V . If the energy V electron volts is sufficiently above the energy of the fundamental absorption edge the electron could, even after losing energy by collisions with the lattice of the impurity host, still retain enough energy to create a new hole electron pair. Thus a single photon absorption would result in two units of charge traversing the circuit making α for the single process equal to 2. Processes of charge multiplication seem to be obscured in a good diode since α approaches unity and is less than unity.

The power P_0 delivered to a matched load R can be written as

$$P_0 = \frac{(q\alpha F)^2 R}{4}$$

This formula is arrived at by assuming that the load resistance R is made equal to the shunt resistance of the generator \mathcal{V} in the equivalent circuit for the photo diode. The result is true at low frequencies where the shunt capacitance of the diode is ineffective. The shunt capacitance in the equivalent circuit represents the incremental depletion capacitance of the junction.

For the case of interest where $R \ll Y$ and the frequency is low enough that the junction capacitance is ineffective

$$P_o = (q\alpha F)^2 R$$

We will turn our attention to the frequency response of a broad band diode photodetector. Given a load R , and a desired band pass of upper frequency f , the junction capacitance C must be designed to meet the requirement

$$C \ll \frac{1}{2\pi f R}$$

The junction thickness is a parameter of primary importance since it will determine the time necessary for a charge carrier to traverse it. The transit time of the carrier must be small compared with the reciprocal of the frequency being detected preventing the serious phase shifts that would occur if this was not the case. If this frequency is g , the optimum barrier width Y will be given by

$$Y = \frac{v}{2\pi g}$$

where g is the response frequency of the detector and v is the drift velocity of the carriers in the junction. v saturates at a value approximately equal to 10^7 cm/sec. for semiconductors, and increases to this value as the bias voltage is increased.

Note that the barrier thickness is made as wide as possible consistent with transit time requirements, thus allowing the smallest junction capacitance to exist in a given design situation. A design carried out in this manner will optimize bandwidth for a given load. Operation with a high reverse bias is desirable in order that the barrier thickness can

be extended, while keeping the transit time as a desired value. The increase in barrier width will lower the junction capacitance and so extend the bandwidth.

We have established that the detector will respond to a frequency g determined by transit time considerations. The bandwidth at this frequency is given by:

$$f = \frac{1}{2\pi RC}$$

The response frequency g is selected by shunting the load with an inductance which will resonate with the junction capacitance C at the frequency g .

If we assume that the capacitance is given by

$$C = \epsilon \frac{A}{Y} \quad \epsilon \text{ is the dielectric constant of the medium.}$$

Then we can write from the band width requirement

$$A \leq \frac{Y}{2\pi f R} = \frac{v}{4\pi^2 g f R}$$

This together with the equation

$$Y = \frac{v}{2\pi g}$$

determines the dimensions of the junction. The design is optimum if the bias voltage is made large enough so that v is the saturated drift velocity of the carriers in the junction.

From an optical point of view the absorption constant should exceed $\frac{1}{Y}$ in order that an appreciable number of photons may be absorbed in the barrier region (63% if the absorption constant equals $\frac{1}{Y}$).

The diode detector is capable of detecting signals of bandwidth f centred at a frequency g . g is determined by the barrier width and by the drift velocity of the charge carriers in the junction. The bandwidth is determined by the area of the junction, the drift velocity, the load and the centre frequency g .

We will now deal with the mixing process in a square law detector. Consider two similarly polarized beams of coherent light of slightly different frequency. Assume these beams to be spatially coincident on the photosensitive surface of a solid state photodiode. The number of hole-electron pairs is proportional to the square of the electric field vector. Let the magnitudes of the electric field vectors be E_1 and E_2 and the frequency of the radiation be ω_1 and ω_2 . Let β be the optical absorption constant. Then the number of hole electron pairs $N(z)$ produced at a distance z from the surface of the semiconductor is given by:

$$N(z) \propto \left[(E_1 \cos \omega_1 t + E_2 \cos \omega_2 t) e^{-\beta z} \right]^2$$

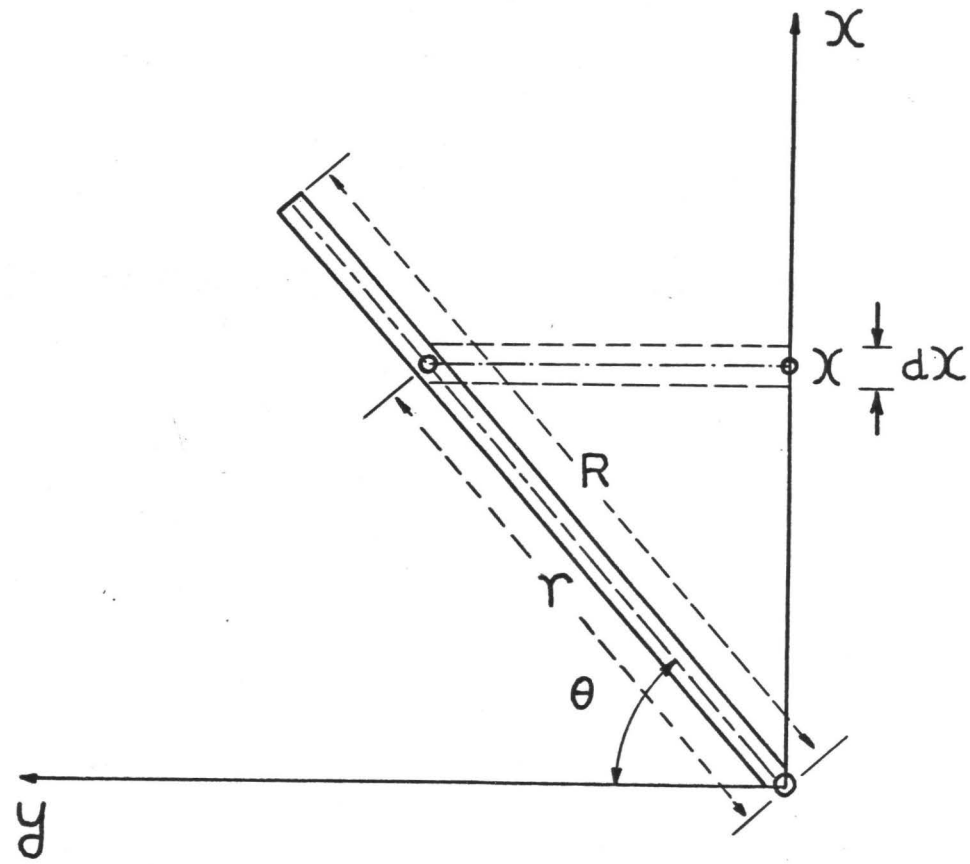
Expanding and using some trigonometric relationships we find:

$$N(z) \propto \left[\frac{E_1^2}{2} + \frac{E_2^2}{2} + E_1 E_2 \cos(\omega_1 - \omega_2)t + E_1 E_2 \cos(\omega_1 + \omega_2)t + \frac{E_1^2}{2} \cos 2\omega_1 t + \frac{E_2^2}{2} \cos 2\omega_2 t \right] e^{-2\beta z}$$

Since ω_1 and ω_2 are optical frequencies, terms containing $\omega_1 + \omega_2$, $2\omega_1$, $2\omega_2$ can be neglected.

The number of hole electron pairs created will then consist of two distinct terms. A DC term given by

$$N_{DC} = \frac{1}{2} (E_1^2 + E_2^2) e^{-2\beta z}$$



GEOMETRY USED TO CALCULATE THE EFFECT OF DETECTOR TILT ON THE BEAT FREQUENCY OUTPUT

FIGURE 4.6

and a difference frequency term given by

$$N_{\Delta\omega}(z) = E_1 E_2 \cos \Delta\omega t e^{-2/\beta z} \quad \Delta\omega = \omega_1 - \omega_2$$

If the difference frequency $\Delta\omega$ falls within the band width of the detector it can be extracted electronically if the signal is above the noise.

The mathematics is identical to that which would arise in the description of the detection of a chopped light beam in the presence of a DC background.

We note that it is desirable to have the absorbing region of the order $\frac{1}{\beta}$ and that the transit time of the light through the absorbing region must be small compared with the reciprocal of the beat frequency. The latter consideration need not concern us.

In the previous paragraphs we considered the case of normal incidence. We will now deal with the case of oblique incidence and show that detector alignment relative to the incident beam is not a problem for beat frequencies in the range 0-60 Mc.

We choose a point in space where the two coincident plane waves are exactly in phase. Call this point $y = 0$. We can assume without loss of generality that this point lies as shown in the diagram. The net wave is the sum of the contributions of each individual wave. We write accordingly:

$$E_T = E_1 \cos(\omega_1 t - \kappa_1 y) + E_2 \cos(\omega_2 t - \kappa_2 y)$$

The surfaces of constant phase are plane and are given by $y = \text{constant}$.

The spatial equation of the absorbing region of the detector is given by:

$$y = r \cos \theta \quad \theta = \text{constant}$$

Thus E_T along the absorbing region is:

$$E_T = E_1 \cos(\omega_1 t - K_1 r \cos \theta) + E_2 \cos(\omega_2 t - K_2 r \cos \theta)$$

The number of hole-electron pairs released at point r in a strip of width dr is given by:

$$dN(r) \propto [E_T]^2 \sin \theta dr$$

$$dN(r) \propto \left[\frac{E_1^2}{2} + \frac{E_2^2}{2} + E_1 E_2 \cos[(\omega_1 - \omega_2)t + r \cos \theta (K_2 - K_1)] + \text{optical terms} \right] \sin \theta dr$$

Therefore summing the contributions along the whole detector length we get:

$$N(R) = \int_0^R dN(r) \doteq \left[\frac{E_1^2 + E_2^2}{2} \right] \sin \theta R + \left[\frac{E_1 E_2 \sin[\Delta \omega t + r \cos \theta \Delta K]}{\cos \theta \Delta K} \right] \sin \theta \Big|_0^R$$

$$N(R) \doteq \left[\frac{E_1^2 + E_2^2}{2} \right] \sin \theta R + \frac{E_1 E_2 \sin \theta}{\cos \theta \Delta K} \left[\sin(\Delta \omega t + R \cos \theta \Delta K) - \sin \Delta \omega t \right]$$

For the case where $R \cos \theta \Delta K \ll 1$

$$N(R) \doteq \left(\frac{E_1^2}{2} + \frac{E_2^2}{2} + E_1 E_2 \cos \Delta \omega t \right) R \sin \theta$$

$R \cos \theta (K_2 - K_1) \ll 1$ in our case because $R(K_2 - K_1) \ll 1$ for the range (8 to 60 Mc). Normal incidence is thus not critical for detection of beat frequencies in this range. It is desirable to have roughly normal incidence to maximize $\sin \theta$.

The condition for successful detection of beat signals then becomes:

$$R(K_2 - K_1) \ll 1 \quad \text{or} \quad R \ll \frac{C}{\Delta f}$$

C = speed of light in the junction

Δf = beat frequency of interest

R = detector dimension.

For beat frequencies of 60 Mc and lower we see angular alignment considerations are far from critical. This result has been verified experimentally.

4.4 Electronics

a) Wide band amplifier

The wide band amplifier used in the experiments on beat frequencies was an Aremberg Ultrasonics Model #WA-600-C with a band pass of 2-60 Mc. The maximum gain was measured and found to be 60 ± 5 db within the band pass. With the gain setting at maximum gain, noise from the first stage was found to almost completely saturate the output. The amplification is attained by using 11 stages of 6AK5 tube amplification. The output from the amplifier is taken off the plate of a 6AH6 tube. Each stage of amplification has a nominal gain of 5.5 db and a band width of 70^{Mc} db. The output of the

plate of the 6AH6 can be further amplified by another stage of 6AH6 amplification. The signal will then be rectified by a diode bridge circuit. The output from the bridge circuit is then amplified by a pulse amplifier capable of responding to a 10 Mc signal. The output from the pulse amplifier, termed the Video output, is present when a fast burst of RF is fed into the input and the video section of the wide band amplifier is turned on. Thus the video section of the amplifier can be used to detect the presence of RF at the input of the wide band amplifier by simply monitoring the tell-tale video output pulse.

b) Filter

In order to remove the "DC level" from the signal fed into the wide band amplifier input a filter stage was designed. Laser pulses are typically 1 to 0.5 microseconds wide. For a quick analysis we can assume that the pulse is Gaussian in shape and write its amplitude as a function of time $f(t)$ as:

$$f(t) = e^{-pt^2} \quad (13)$$

Thus the pulse has unit amplitude at $t = 0$ where it also takes on its maximum amplitude.

To look at the frequency spectrum of the pulse we take the Fourier transform of the amplitude function. Thus we write

$$F(\omega) = \frac{1}{\sqrt{2\pi}} \int_{-\infty}^{\infty} e^{j\omega t} f(t) dt = \frac{1}{\sqrt{2p}} e^{-\omega^2/4p}$$

At $\omega = \omega_0 = 2/\sqrt{p}$ the frequency content is down to $\frac{1}{e}$ of the maximum frequency content which is at $\omega = 0$.



THE WIDE BAND AMPLIFIER

FIGURE 4.7

We consider the case of a pulse with a width of 0.25μ seconds.

We can solve for p from (13):

$$P = 64 \times 10^{12} \text{ sec}^{-2}$$

Therefore, $\omega = \omega_0 = 16 \times 10^6$ radians/sec. $f_0 = 2.55$ Mc.

$$\left. \begin{array}{l} \text{at } \omega = 2\omega_0 \\ f = 2f_0 \\ = 5.1 \text{ Mc} \end{array} \right\} \sqrt{2p} F(\omega) = \frac{1}{e^4} = 0.0183$$

Thus the frequency content at 5Mc is down to 1/50th of the DC content, and at 2.5 Mc the content is down to $\frac{1}{3}$ of the DC content.

Consider a signal defined by

$$\begin{aligned} f(t) &= \cos \omega_1 t \cos \omega_2 t & \omega_1 |t| \leq \frac{\pi}{2} \\ f(t) &= 0 & \omega_1 |t| \geq \frac{\pi}{2} \end{aligned} \quad \omega_2 \gg \omega_1$$

This function is used to represent the approximate form of the modulation found on a spike from a ruby laser.

To find the frequency spectrum of such a signal we write:

$$2 \cos \omega_1 t \cos \omega_2 t = \cos(\omega_1 - \omega_2)t + \cos(\omega_1 + \omega_2)t$$

We now proceed to calculate the Fourier transform of the signal.

The Fourier transform of the signal is given by:

$$\begin{aligned} F(\omega) &= \sqrt{\frac{2}{\pi}} \int_0^{\pi/2\omega_1} [\cos(\omega_1 - \omega_2)t + \cos(\omega_1 + \omega_2)t] \cos \omega t dt \\ &= \sqrt{\frac{2}{\pi}} \frac{\sin(\omega_1 - \omega_2 - \omega)t}{2(\omega_1 - \omega_2 - \omega)} \Big|_0^{\pi/2\omega_1} + \sqrt{\frac{2}{\pi}} \frac{\sin(\omega_1 - \omega_2 + \omega)t}{2(\omega_1 - \omega_2 + \omega)} \Big|_0^{\pi/2\omega_1} \\ &\quad + \text{terms due to } \cos(\omega_1 + \omega_2)t \end{aligned}$$

Now consider

$$\frac{\sin(\omega_1 - \omega_2 + \omega) \pi/2\omega_1}{2(\omega_1 - \omega_2 - \omega)} \quad (14)$$

$$\text{Let } \omega_2 - \omega_1 = \Delta\omega \doteq \omega_2$$

Hence we can write (14) as:

$$\frac{\sin(\omega - \Delta\omega)\pi/2\omega_1}{2(\omega - \Delta\omega)}$$

This function has a peak of magnitude $\frac{\pi}{4\omega_1}$ at $\omega = \Delta\omega$

A second negative peak occurs when

$$\omega = \Delta\omega + 3\omega_1$$

it has magnitude $-\frac{1}{6\omega_1}$

It is down to approximately one fifth the value of the maximum peak.

We have shown that a modulation of the form:

$$\cos\omega_1 t \cos\omega_2 t$$

will give rise in positive frequency space to two main "peaks" with half-width of the order of ω_1 . One of these peaks is centred at $\omega = \omega_2 - \omega_1$, the other is centred at $\omega = \omega_2 + \omega_1$.

The modulated laser pulse can be represented approximately by the function:

$$f(t) = A e^{-pt^2} + B \cos\omega_1 t \cos\omega_2 t \quad |\omega_1 t| \leq \frac{\pi}{2}$$

$$A \gg B, \quad \omega_1 \ll \omega_2$$

$$f(t) = A e^{-pt^2} \quad |\omega_1 t| \geq \frac{\pi}{2}$$

$$T_0 = \frac{2}{\sqrt{p}}$$

$$\omega_1 T_0 = \frac{\pi}{2}$$

Therefore

$$\omega_1 = \frac{\pi}{4} \sqrt{p}$$

In frequency space we have approximately:

$$F(\omega) = \frac{A}{\sqrt{2p}} e^{-\frac{\omega^2}{4p}} + \frac{B}{2} \sqrt{\frac{2}{p\pi}}$$

+ (negligible term due to the second peak at $\omega = \omega_2 - \omega_1$)

$$\text{for } \omega = \omega_1 + \omega_2 \doteq \omega_2$$

If $A = 100B$ it is evident that the modulation will give a unity signal to (DC) "noise" ratio at $\omega_2 \doteq \omega_0$ when

$$\frac{A}{\sqrt{2p}} e^{-\frac{\omega_0^2}{4p}} = \frac{B}{2} \sqrt{\frac{2}{p\pi}}$$

$$\text{or } \log_e \sqrt{\pi} 10 = \frac{\omega_0^2}{4p}$$

$$\omega_0^2 = 4p \times 3.45$$

$$f_0 = \frac{\omega_0}{2\pi} \doteq 5.1 \text{ Mc}$$

if $p = 64 \times 10^{12}$ (corresponding to a laser pulse of width 0.25μ seconds).

Bearing in mind calculations of the above type a filter section was designed. The filter was of the high pass type with a cut-off at 8.3Mc . It consisted of 3 sections, a central T section and two L sections. The nominal terminating impedance was 93ohms . Inserting the filter in the input of the wide band amplifier, which has a 93ohm input impedance, and testing the compound unit showed that no significant standing wave patterns in the gain profile of the amplifier were produced by the filter.

Under operating conditions the filter was found to be satisfactory and clean R.F. signals were obtained from the output of the wide band amplifier, undistorted by the DC level of the laser output pulse.

4.5 Experimental Arrangement

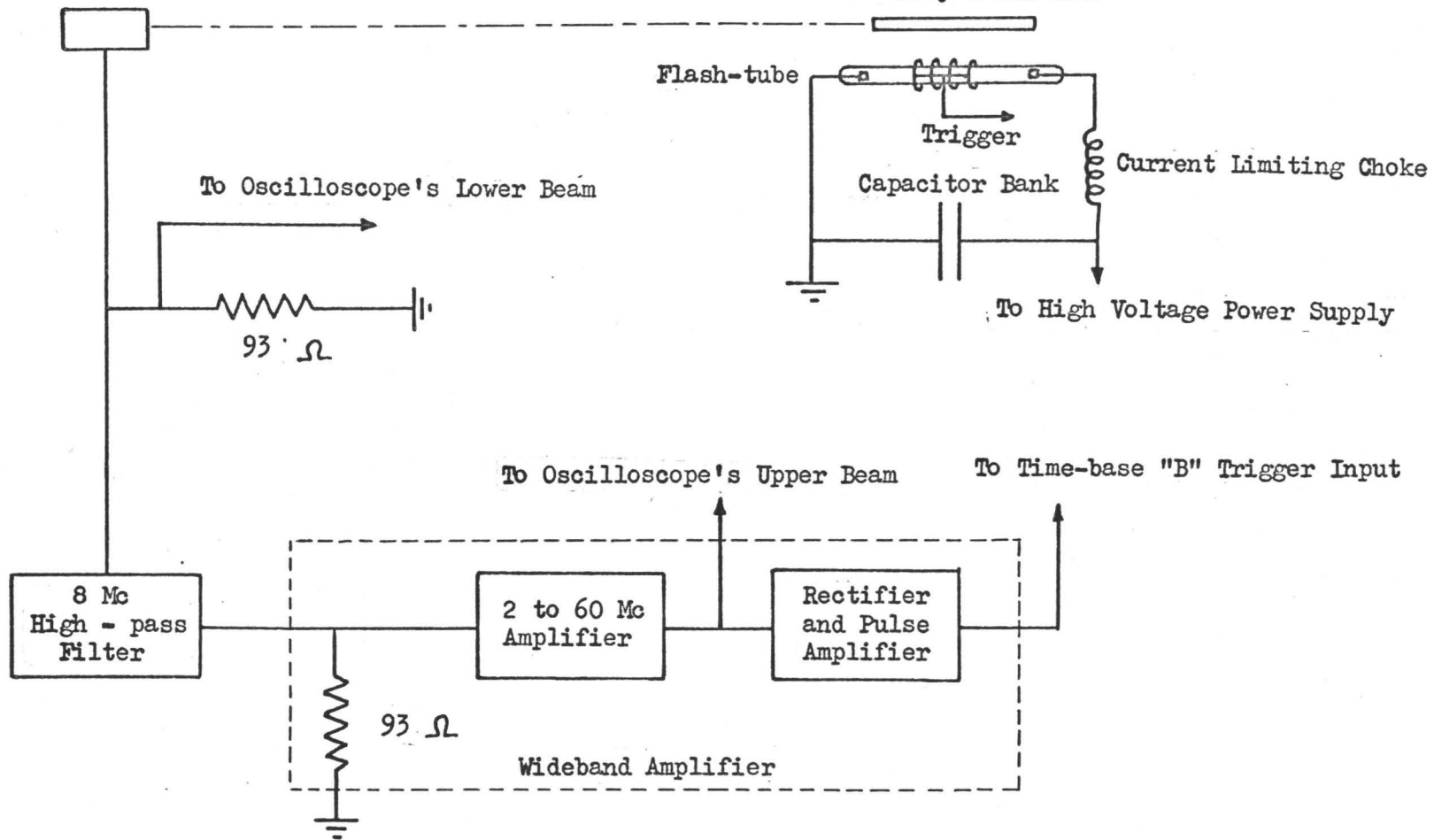
The experimental arrangement for the detection of the beat frequency signals consisted of a square law diode detector. The signal generated by incident laser light was taken from a 100 Ω load and fed into the lower beam of a Tektronic 555 dual beam oscilloscope. The same signal was tapped at the 100 Ω load and fed into 93 Ω coaxial cable leading to the high pass filter which was terminated by the 93 Ω input impedance of the Wide Band Amplifier. The RF output from the wide band amplifier was fed to the upper beam vertical deflection preamplifier of the Tektronic 555 scope. The plug in unit used was the Tektronic Model A. It was found that the other available plug in unit type H although having higher sensitivity, tailed off noticeably at about 30Mc and was hence judged unsuitable to detect the beat frequencies. Type A however, was found to have a high enough cut-off to do the job. It tailed off noticeably at about 50Mc.

The high frequency response of the oscilloscope though not suitable for quantitative amplitude measurements at the high frequencies under observation was nevertheless sufficient for the measurement of frequency in the range (8-60Mc). This of course is evident, since interest was concentrated on the behaviour of the beat frequencies in a ruby laser rather than the relative amplitudes of these beats.

To avoid frequency selection based on the response of the electronics, the scope was triggered from the video output of the wide band amplifier. Since the 555 Tektronic scope is provided with two time base units and each trace can be swept with either time base unit, it was con-

Back Biased Diode Detector

Clad Ruby Laser Rod



SCHEMATIC DIAGRAM OF THE BEAT FREQUENCY DETECTION APPARATUS

FIGURE 4.8

venient to trigger the first time base instantaneously with the laser flashtube, and at the same time keeping both beams coupled with a second time base unit. A mode of operation of the scope permits the user to trigger the first time base unit and after a pre-set delay time, the second time base unit is automatically made "Ready" to receive an activating trigger pulse which may come at any time after the pre-set delay time. The pulse used to trigger the second time base unit was provided by the video output of the wide band amplifier. The pre-set delay time was selected to make the second time base unit triggerable after the start of lasing. As soon as a modulation of sufficiently high amplitude was sensed by the wide band amplifier, a pulse from the video amplifier would trigger the second time base unit - allowing photographs of the modulation and the pulse to be taken as they appeared simultaneously on the oscilloscope trace.

CHAPTER 5

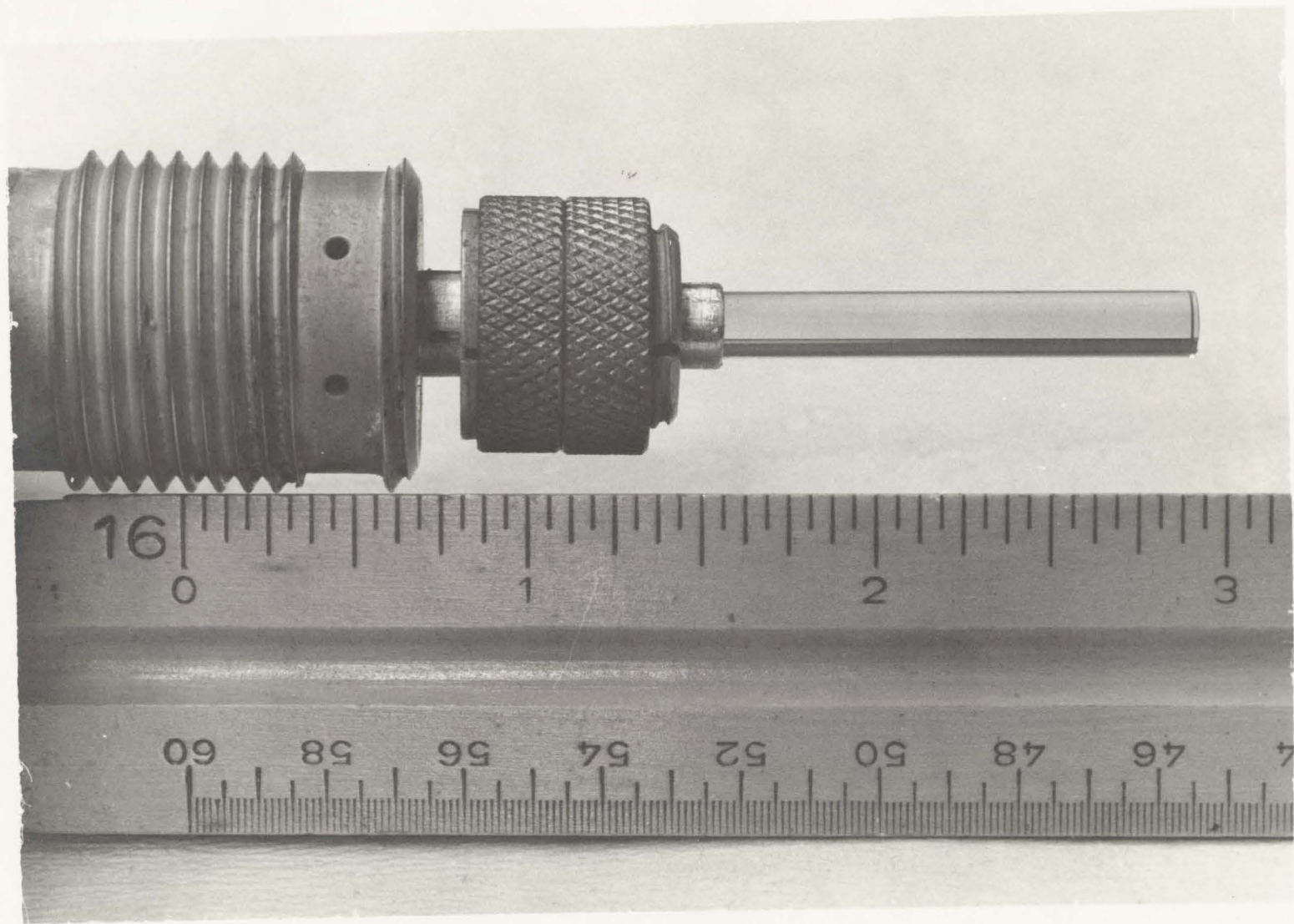
EXPERIMENTAL METHOD

5.1 Selection of the Sapphire Clad Ruby

For the experiments on beat frequencies a sapphire clad ruby laser rod was chosen. Several considerations led to this choice. It is desirable in experiments on beat frequencies to try to keep distortion of the cavity dimensions caused by thermal expansion of the laser medium to a minimum. Lasers with a low threshold will need a pump of lower energy than lasers of high threshold. Now, since lasers absorb a photon of relatively high energy for every lower energy photon that they emit coherently, it is evident that part of the pump source energy absorbed by the active laser material will appear as heat in the crystal host. Any improvement in laser threshold will hence minimize the amount of heat appearing in the laser medium and in so doing lower strains in the medium, and hence distortions of the laser cavity, during pump excitation.

The possibility of extracting heat rapidly from the laser medium is highly desirable and in this respect ruby and sapphire are ideal specially at low temperatures where their thermal conductivity is high. (For instance, the thermal conductivity of sapphire reaches a peak of around 60 watts/cm^{°K}.) The faster heat can be extracted from the laser medium as it is created there by the high pump intensities, the lower will be the temperature rise of the medium during excitation and lasing.

The heat capacity of the medium and the magnitude of the coefficient of thermal expansion will also play an important role in determining cavity deformation under the action of pump light.



THE CLAD RUBY IN THE HOLDER

FIGURE 5.1

Given a laser medium it is possible to improve its threshold by physical means while at the same time improving considerably the chances of removing heat from the active medium rapidly. This can be done by cladding the cylindrical sample of laser material with a jacket of the same index of refraction as the material. The jacket is chosen to transmit, without attenuation, the useful pumping light frequencies that invert the population of the active ions. Directing our attention to a ruby laser, an improvement in threshold can be obtained by cladding the ruby core with a sapphire sheath. The radius of the core and sheath will be shown to be related for optimum pumping conditions. Ruby and sapphire have essentially the same physical properties. Their indices of refraction are almost identical as are their thermal conductivities, so sapphire is an ideal choice as a cladding host.

A ray which is tangential to the cladding-space interface will pass tangentially to an inner cylinder of radius $\frac{R}{n}$, where R is the radius of the cladding and n is the index of refraction of the cladding medium. (1.76 for sapphire.) This result is true as long as the ray under consideration travels within a plane whose unit normal is parallel to the axis of the cylindrical rod.

Thus it is seen that if every point on the surface of the cladding is illuminated with pump light rays in such a way that the paths of these rays always travel in a plane whose unit normal is parallel to the axis of the cylindrical rod, and whose distribution is such that all angles of incidence of the pump light are equally likely in a given plane, then the central core of radius $\frac{R}{n}$ will be uniformly illuminated.

In a clad ruby, the light is gathered by a rod with dimensions of the cladding but concentrated and used by a rod with dimensions of the core. The result is a lowering of the oscillation threshold. Heat from the activated core is transmitted rapidly to the surface of the cladding at low temperatures, since sapphire and ruby have a thermal conductivity equal to that of copper when the former materials are at 77°K. Heat transfer is in this case boundary limited and is expected to take place faster by a factor given by the index of refraction of the cladding and core, since this is the effective increase in the heat transfer area of the rod (neglecting end effects).

Let us recall to mind the basic formulation of the theory of modes as proposed by Fox and Li. The model employed for the integral equation representation of modes in a laser resonator is that of two end reflectors facing each other forming a laser cavity. The light wave initially launched at one mirror is assumed to be plane polarized.

In order to comply as rigorously as possible with the physical characteristics of the Fox and Li model a clad ruby was chosen. The C axis of the ruby crystal employed was chosen to be at 90° to the cylinder axis. Experiment has shown that the coherent output of such a crystal is almost entirely plane polarized at low powers. Thus any modes existing in the clad ruby rod would have to be plane polarized and so comply with the model requirements. Off-axis rays that could exist in an ordinary laser rod are minimized in a clad ruby laser rod because such rays would travel mainly through the sapphire of the clad ruby before being reflected at the sapphire-space interface. Thus they are not amplified

sufficiently to exist at low input pump powers. A clad ruby then, satisfies the polarization criteria as well as the boundary criteria employed in the Fox and Li Formulation for modes in a plane parallel laser resonator.

The disadvantage of a clad ruby over a conventional rod is that the lasing region is of the size of the core and would thus not be suited for experiments requiring a somewhat wider beam. (Diameter of ruby core = 80 thousands of an inch; diameter of a conventional ruby = $1/4$ of an inch.)

However, preliminary experiments employing a conventional $1/4$ " rod showed that a maximum active diameter of 80 thou would be suitable for study.

Selecting a small active region of the order of magnitude reported for filamentary lasing in conventional rods, assures that the entire region defined by the end mirrors will lase. Thus the lasing region of an optical resonator is determined by the diameter of the end mirrors forming the cavity if these are less than 80 thou.

Threshold and cooling considerations as well as conformity with the Fox and Li model led to a choice of a clad ruby rod for the final experiments on the beat frequencies of a ruby laser light activated optical resonator. As measured in terms of the agreement between experiment and theory it is concluded that the sapphire clad ruby rod successfully performed to expectations.

5.2 Cooling of Sapphire Clad Ruby Crystal

Cooling a laser crystal provides a challenging problem. The problem consists of attaining reasonably low temperatures while at the same time avoiding entirely the ever present threat of "frosting up" the whole system. The system chosen must, if possible, be of the type that is easy to set into operation with a minimum expenditure of time. The temperatures attainable must be reproducible with a minimum effort. The system must not introduce index of refraction changes between the pump flashtube and the crystal being pumped, in order to avoid unnecessary pump light reflections at the boundaries that would result in having to increase the output energy of the pump to assure lasing. The system decided upon might be required to attain a range of temperatures between room temperature and a minimum operating temperature to add to the system's versatility. It would be highly desirable if the system could be designed to require little if any attention while performing experimental runs.

Keeping in mind the design criteria outlined above a system was chosen and put into operation which represented the best compromise regarding desirable features.

The method of cooling the crystal selected was that of conduction supplemented by lowering the ambient temperature of the crystal. A room temperature crystal chuck was modified to allow crystal temperatures of 77°K to be approached. The cryogenic chuck, as put into operation, consisted of a liquid nitrogen aluminum container surrounded by insulating foam. The aluminum container was soldered to the aluminum chuck using a special solder. The heat transfer area between the liquid nitrogen

and the cylindrical crystal chuck is approximately 3 in.². The crystal chuck screwed into a teflon receptacle which in turn was attached directly to the elliptical housing. Teflon was chosen because of its machinability and its low coefficient of heat transfer. When the chuck was secure in its teflon holder the crystal was held parallel to the linear flashtube and in the second focus of the elliptical laser head by the four grips at the end of the chuck, whose pressure on the crystal end could be adjusted. The chuck was hollow to allow passage of the laser beam. Apertures were present in the chuck to allow cool nitrogen gas to circulate freely around the crystal and then be exhausted to the atmosphere after passage through the apertures and the hollow core of the chuck cylinder. A cool nitrogen atmosphere was provided for the system by evaporating nitrogen gas from a liquid nitrogen dewar, using a simple resistive heater immersed in the dewar. As the current through the heater is increased an increase in the flow rate of nitrogen gas is observed. The evaporated cool nitrogen gas serves two purposes. It mainly provides a dry atmosphere within the elliptical laser head. When cooling is in progress, the entire laser head reaches the dew point of the laboratory air in a matter of a few minutes, so the entire system becomes externally covered with frost. The interior, however, since it is filled with a dry nitrogen atmosphere, remains free of frost. The other function of the nitrogen gas is to reduce the ambient temperature of the crystal and thus remove a significant cooling load from the liquid nitrogen tank circuit.

When the system was in operation the liquid nitrogen tank needed refilling every 10 minutes. The practice however was to top the tank up every minute and a half, to insure temperature stability. In this time interval the laser was activated three times at a uniform rate of one shot every thirty seconds. The temperature of the ruby rod that was attainable using the system was estimated at 85-90°K.

Two liquid nitrogen dewars were necessary to operate the cooling system. One is employed as a storage dewar for use in topping the liquid nitrogen tank. The other is incorporated in the system and is used as a source of cool nitrogen vapour. The heat of evaporation being provided by a resistive heater.

The cool nitrogen gas is used not only to provide a cool ambient temperature for the crystal but also to cool the flashtube. Operation of Xenon flashtubes at temperatures as low as 77°K produces no detrimental effects on the flashtube. Hence cooling the flashtube with the same atmosphere as that used to surround the crystal was found to be a convenient method of attacking the problem.

Cooling the crystal accomplished one primary need as well as a beneficial secondary effect. Firstly cooling the crystal narrows the fluorescent line width of the ruby red line. Thus the gain profile for lasing is narrowed, lowering the number of longitudinal modes that can go unstable. Ideally, it would have been desirable to maintain only one longitudinal mode in oscillation. Secondly, the threshold for relaxation oscillations is lowered with its consequent beneficial effects on cavity stability.

5.3 Experimental Criteria

A useful experimental observable of a laser system is the threshold energy for laser action. The threshold energy is a complex function of several parameters of the system. It depends on the active ion impurity and on the type of host material employed in fabricating the laser rod. Thus present state of the art Nd in glass laser rods has a higher threshold energy for laser action than rods consisting of Nd in a Calcium Tungstate lattice. Threshold is also dependent on the energy level distribution and number of energy levels involved in the dynamics used to obtain a population inversion. Thus Nd in Ca Tungstate has generally a lower threshold than ruby. This experimental observation can be explained if we note that Nd in Ca Tungstate is essentially a 4-level system whereas Chromium in aluminum oxide is a 3-level system. At operating temperatures the terminal level of the Neodinium system lies well above the ground state and so is almost completely depopulated. In the case of ruby, being a 3-level system, the ground state is the terminal level for laser action and so will always contain some ions. Thus a population inversion is much easier to obtain using a Nd rod rather than a ruby rod. Hence threshold will be lower in a Neodinium rod, all other effects being neglected. Since host imperfections (fused layers, seed crystals necessary to control orientation during growth, entrapped gases and lineage, in ruby) tend to broaden the fluorescent line width of the entrapped active ions, as well as act as scattering centers, it is not unreasonable to expect that a laser rod with relatively large quantities of imperfections should exhibit a much increased threshold over an equivalent, but less imperfect rod.

Since lowering the temperature of operation of a laser system generally reduces the fluorescent line width of the active ions, the threshold for laser action is lowered appropriately.

The geometry of the pumping system also has a marked effect on laser threshold. Generally, pump light can be coupled more efficiently into the laser rod by using elliptical geometry as opposed to cylindrical geometry. Laser threshold is thus reduced considerably by using an elliptical laser head. In the experiments carried out on the detection of heat frequencies between active transverse modes, an elliptical laser head and a state of the art ruby rod were used.

The procedure employed to set the pump power in these experiments was as follows. The clad ruby rod was allowed to reach its equilibrium temperature (in the vicinity of 85°K). Threshold was determined by collecting the laser output light with a convex lens and focusing it on the solid state diode detector. The focused spot could be easily seen on a white card placed immediately in front of the diode detector. Detection took place approximately one meter away from the laser rod. In this way leakage light from the pump did not introduce a noticeable DC level in the detected signal. The use of a narrow-band interference filter, peaking at the ruby red line, was thus not required to reject stray pump light. Use was made of the narrow beam quality of the laser output to discriminate against unwanted background.

Once threshold had been determined (in the vicinity of 300 joules) the pump was adjusted to a value above threshold in such a way that a reasonable number of transverse mode beat frequency signals were detected.

This was determined by viewing the laser output as well as the time coincident video amplifier output on a dual beam oscilloscope (Tecktronic 555). A "reasonable" number of beat frequencies is defined roughly as one beat signal for each four spikes on the trace. It was generally necessary to go about 5 or 10% above threshold before this condition was met. The adjustment in pump output energy at times resulted in a considerable increase in coherent output power from the laser rod. It was thus necessary, in order to avoid overdriving the diode detector, to remove the focusing lens and even attenuate the laser beam with several neutral density filters.

Once it had been established that a sufficient number of transverse modes were oscillating during lasing as determined by observing the output from the video amplifier, the delay of the time base unit deflecting both beams of the dual beam oscilloscope was modified. The sweep was made "ready to be triggerable" after approximately 0.7 millisecond had evolved from the start of pump excitation of the crystal. This corresponded to a time when 60% of the train of laser pulses had already evolved. It was thus possible to sample beat frequencies of the last 40% of the laser pulse train. The sampling was random in the sense that no frequency-selective mechanism was employed for triggering the trace. The only criterion necessary was the existence of a beat frequency which would produce a video pulse large enough to trigger the time base unit of the oscilloscope. It was reasoned that toward the end of lasing a larger minimum flux density existed and thus lower order modes could establish themselves without interruption. Analytical solutions to the rate equations show that the minimum value of the flux density occurs approximately equally spaced from

two adjacent maxima and is critically dependent on the mean of the two adjacent maxima.

The choice of Fresnel number for the cavity dimensions requires consideration. A large Fresnel number means that beat frequencies between transverse modes will be generally lower than those detected from a cavity whose Fresnel number is smaller. The larger the Fresnel number, the lower will be the diffraction losses associated with a particular mode of oscillation. Mode selection is expected to take place only if the diffraction losses predominate over other losses in the system. These considerations lead to a choice of a moderate Fresnel number for experiments on beat frequencies. The Fresnel number must be such that beat frequencies between a few of the low order modes fall within the range of detection (8-60 Mc) but other beat frequencies fall above the highest frequency detectable by the electronics. The Fresnel number must not be so small that only the lowest order (least lossy mode) mode breaks into oscillation because then no beats would be detectable. If the Fresnel is $a^2/b\lambda$

a = radius of cavity

b = length of cavity

λ = wavelength of oscillation

for a cavity formed by two circular mirrors of equal radius " a " and facing each other then the Fresnel number of a cavity formed on the same crystal by two mirrors one of which has radius " a " and of which the other has a radius much larger than " a " is $a^2/b\lambda^2$.

This simple relationship allows one to silver one face of the laser rod entirely and silver the other end with a small spot of radius "a". The Fresnel number for the cavity is then controlled by the small silver spot radius and critical centering of the two deposited silver spots (which would be quite tedious) is avoided entirely. The above procedure was employed for determining the Fresnel numbers of the various cavities used in this study of beat frequencies.

The Fresnel-number range employed was ($35 \rightarrow 5$) corresponding to radii of 40 to 15 thousands of an inch with $2b = 3$ inches. Computer solutions for the theoretical beat frequencies between the first 45 lowest order modes show that this was a reasonable choice of Fresnel number range. Inclusion of the first 45 lowest order modes does not change the frequency spectrum, calculated on the basis of low order modes, appreciably at the low frequency end of the spectrum where observations took place.

In order not to waste pump excitation energy it is necessary that the duration of the pumping pulse be smaller than the spontaneous lifetime of the material being pumped. For ruby, the spontaneous decay time of the active level is three milliseconds. A pumping pulse of one millisecond was decided upon. This decision is consistent with the pump pulse width requirements as well as with flashtube life considerations. The lifetime of the flashtube is decreased if high and narrow pulses of current are passed through it. Thus a flashtube rated at 500 joules will have a lifetime as specified by the manufacturer only if a current limiting choke of the size suggested by the manufacturer is used. Operation at 500 joules input energy to the flashtube with a choke of lower inductance than that recommended will diminish considerably the flashtube's

inherent long life. When the output light pulse from the flashtube is choke limited the pulse width T can be calculated to be:

$$T = \pi\sqrt{LC}$$

where L is the choke inductance in henries and C is the capacitor bank capacitance in farads. T is then given in seconds.

In these experiments $C = 400 \mu\text{f}$

$L = 400 \mu\text{h}$

T is then 1.25 milliseconds.

The pulse width observed experimentally was of the order predicted above. Operation of a ruby laser at room temperature results in larger and narrower spikes than does operation at liquid nitrogen temperatures. In order to make absolutely sure that the oscillations observed during a laser light output maximum were not due to some form of ringing of the electronics the following experiment was performed. A ruby laser was operated at room temperature and its output analyzed for beats. Although the spikes were narrow few beats were observed, showing that ringing was not responsible for the oscillations. With all apparatus settings undisturbed the rod was operated at liquid nitrogen temperatures. The output was analyzed for beats and showed a prolific number even though the relaxation spikes from the ruby were at least twice as wide and half as high and rose from a "DC level", confirming that electronic ringing was not a factor.

The beats disappear when the light of the laser is blocked away from the diode detector, hence extraneous R.F. coupling was non-existent.

It is concluded beyond doubt that the oscillations observed during the laser spike are due to an inherent property of the light being detected and not to the circumstances under which the light was detected.

5.4 Photographic Synchronization Techniques

The problem of displaying and recording the beat frequencies detected from a clad ruby laser was satisfactorily solved by using a Tecktronic (Type 555) oscilloscope in conjunction with a Polaroid camera. The camera was fitted on a DuMont Mount. The screen of the oscilloscope could be simultaneously viewed and photographed. The camera objective had a maximum aperture setting of f-1.9. This moderately fast objective coupled with the use of extremely fast Polaroid oscilloscope Film (ASA 10000) was found suitable for recording beat frequencies up to about 60 Mc by photographing the beat frequency signal on the oscilloscope's video screen. The fast film was necessary since the screen and beam accelerating potential of the oscilloscope are not optimum for the fast writing speed that is essential in beat frequency recording. The fast film however compensated for the moderate writing speed of the oscilloscope, resulting in acceptable beat frequency photographs.

The dual beam oscilloscope proved convenient in that the beat frequency modulation could be viewed simultaneously with the laser relaxation oscillation spike carrying the modulation. Since the amplitude of the modulation varied considerably from spike to spike a certain combination of gain settings could be chosen that would insure that the modulation was visible on the actual spike when the beat was of suf-

ficient amplitude to overdrive the oscilloscope beam carrying the amplified beat frequency signal. If the beat frequency amplitude carried directly on the relaxation spike happened to be small, it was then possible to make frequency measurements on the recorded output from the wide band amplifier.

This resulted in a larger number of useful photographs and hence a smaller number of wasted shots.

In a typical run the output from the back biased diode detector was monitored directly on one of the oscilloscope's beams. The signal produced by the laser output on the diode junction was also filtered to remove the spike envelope and then amplified. The output of the wide-band amplifier was then fed to the oscilloscope and monitored on the remaining beam. The output of the amplifier was the beat frequency modulation present on the relaxation spike. In order to avoid wasting film by photographing a range of lasing where no beats were present, the video amplifier was used to sense the presence of a strong beat frequency signal. The output of the video amplifier was then used to trigger the time base carrying both oscilloscope traces. In order to record the beat frequency signal and the laser spike, the camera shutter was opened prior to triggering the laser pump flashtube. Sufficient time was allowed for the oscilloscope screen to form an image on the polaroid film.

A statistical picture of the laser beat frequencies was built by taking many photographs of the beat frequency signals for several optical cavity radii.



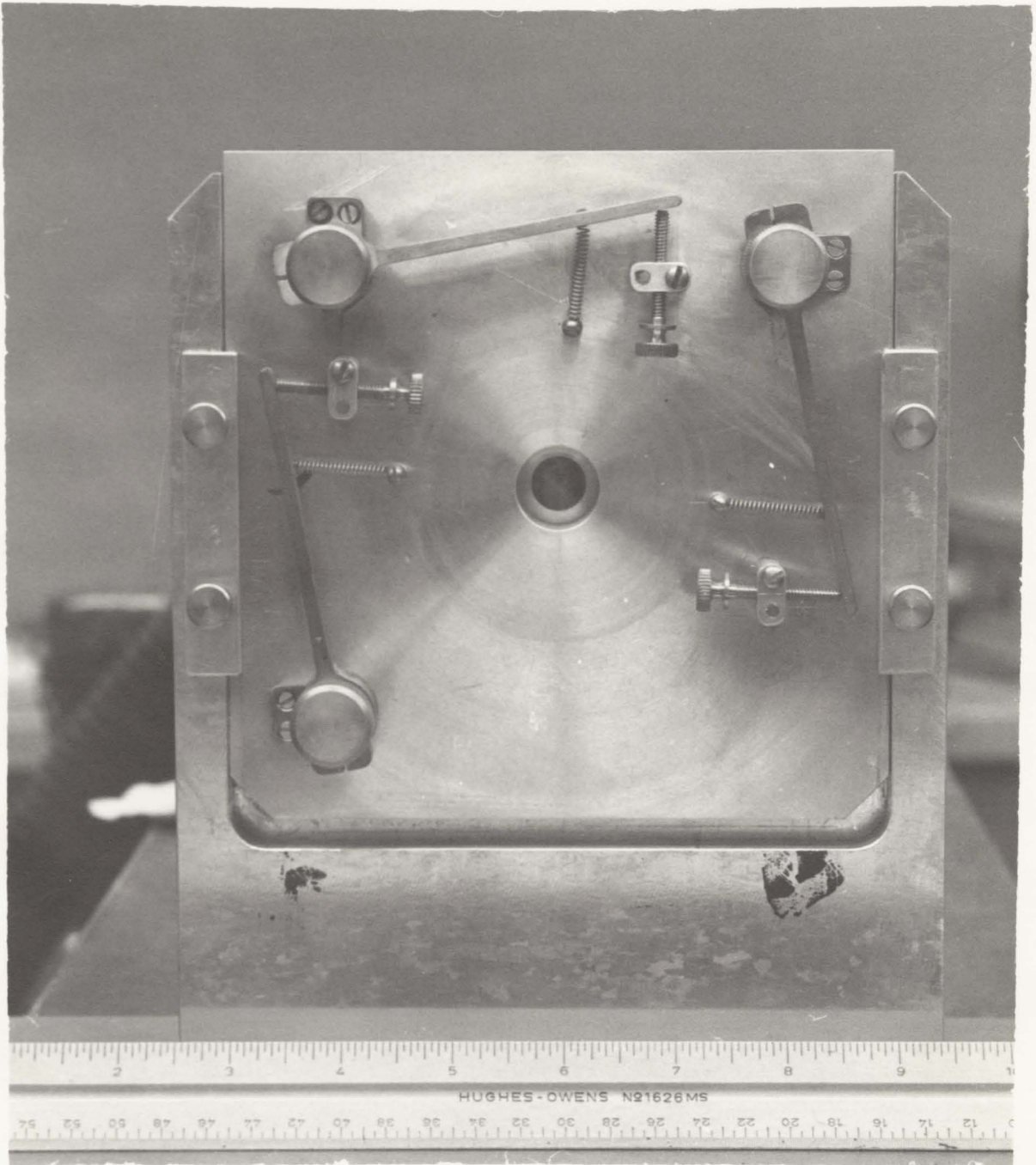
THE CAMERA USED TO RECORD THE BEAT FREQUENCIES

FIGURE 5.2

5.5 Formation of the Optical Cavity by Vacuum Deposition of Silver on the Crystal End Faces

State of the art ruby rods are made of a single Al_2O_3 crystal doped with Chromium whose concentration is generally about .05% by weight. The common crystal geometry employed in ruby laser rods is cylindrical. The end faces of the cylindrical ruby are generally parallel to about five seconds of arc and plane to 1/5th of a wavelength of the ruby red light (6900 A). These tolerances provide a convenient way of forming an optical resonator by depositing thin silver films on the two crystal faces. Alignment of the resonator mirror is thus guaranteed to the tolerances imposed on the crystal end faces. It is possible to form the optical cavity using external mirrors and parallelism of $\frac{1}{2}$ second of arc has been achieved without difficulty in the laboratory at McMaster using external mirrors.

It has been pointed out that when one of the mirrors of the cavity has an area much larger than that of the other mirror then the smaller mirror determines completely the geometry of the effective optical cavity. This geometry is that of two mirrors of the size of the smallest separated by twice the distance between the large mirror and the small mirror of the real cavity. It is thus sufficient to silver one spot of the required radius on one end of the ruby rod and silver the opposing end entirely. The small silver spot then determines the cavity dimensions. The spot size can then be determined using a machinist's microscope which is available to measure distances up to one ten thousandth of an inch. This method was employed to measure the spot sizes of the various cavities used in the beat frequency measurements.



A PRECISION MIRROR HOLDER

FIGURE 5.3

The spot sizes were controlled approximately by silvering the crystal face while the crystal was being held in one of several teflon jigs. These jigs were made to hold the crystal snugly and were provided with an aperture of the require diameter, positioned close to the crystal face. The aperture was centered with the axis of the ruby core. This method of silvering a spot on the crystal end face proved satisfactory. Consistent spot sizes were obtained from each jig and in each case the spots were centered on the ruby core.

The method of depositing the crystal film on the end of the ruby rod will now be described. The technique employed is that of high vacuum deposition. By placing the crystal in a bell jar which can be evacuated, it is possible to deposit a thin silver film onto one or other of the crystal faces. This is accomplished by evaporating a piece of silver wire placed in thermal contact with a molybdenum boat. The boat's temperature is raised by passing a current through it and eventually the silver evaporates. A sufficiently low pressure is maintained within the bell jar to make the mean free path of the evaporated silver atoms large compared to the distance between the ruby crystal and the molybdenum boat. This serves to make true trajectories of the silver atoms. Oxidation of the silver is minimized by working under conditions of low pressure. Impurities of high vapour pressure will tend to be removed from the bell jar by the diffusion pump.

The unit employed to provide the evacuated bell jar and the current source necessary to heat the silver to its evaporating point was an Edwards Model 12E3 Vacuum Coating Unit.

The rotary pump belonging to the unit attains 5×10^{-3} Torr., while the ultimate pressure in the bell jar can be made to reach less than 5×10^{-6} Torr. by using the diffusion pump. Thus, the pressure attained in the bell jar is low enough to easily meet vacuum deposition requirements.

The correct quantity of silver must be evaporated to attain the required resonator mirror reflectivity. Evaporation of 100 mg of silver resulted in a reflectivity close to 100%. Thus 100 mg of silver were evaporated to produce the larger of the two mirrors since it was decided to detect the laser output emanating from the crystal face silvered with the small spot. 45 mg of silver produced reflectivities of about 90% and this is the quantity of silver used to form the small spot of silver whose size was determined by the teflon mask. The transmission of such a film is high enough to allow a sufficient amount of laser output to be coupled to the detector.

CHAPTER 6

RESULTS

It rapidly became apparent that it was not possible to interpret the data gathered from beat frequency measurements on an absolute basis. It was not possible "a priori" to predict the outcome of a given beat frequency measurement. The range of observation (8-60 Mc) could not be assigned discreet frequencies upon any of which any given measurement of a beat frequency must fall. However, by measuring a large number of beat frequencies, a histogram could be constructed showing the relative occurrence of beat frequencies as a function of frequency. The number of beat frequencies in the sample was judged to be large enough to show the gross features of the beat frequency probability distribution. In every case a large majority of the beat frequencies for a given resonator radius fell within a range of about 15 Mc whose center frequency varied with resonator radius. Some rather strong peaks are observed within the 15 Mc range, indicating a tendency for many of the frequency measurements to fall within a Megacycle or two of each other. These peaks are interpreted as being due to a beat between two modes that are favoured to break into oscillation by an arrangement of uncontrolled variables influencing the mode structure of a laser. This uncontrolled favouring mechanism will therefore diminish considerably the chance for some other modes to break into oscillation and hence only a single highly occupied frequency range is expected. Other modes will be at times present in

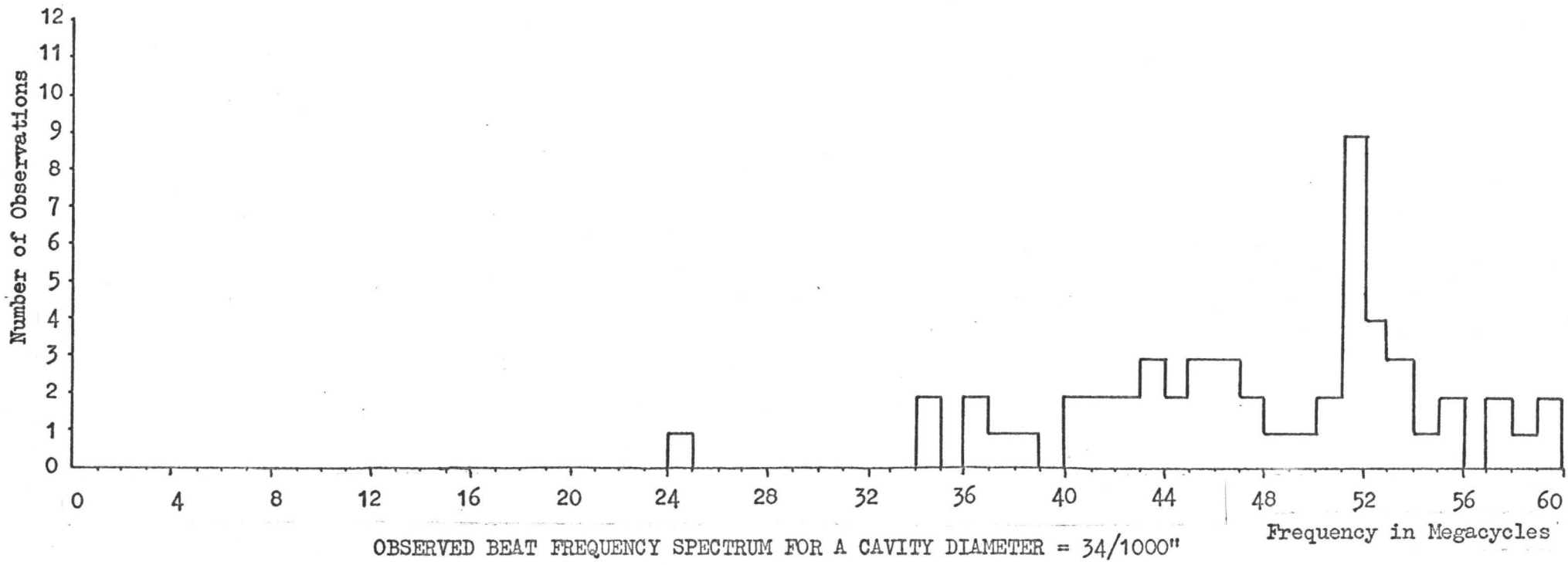


FIGURE 6.1

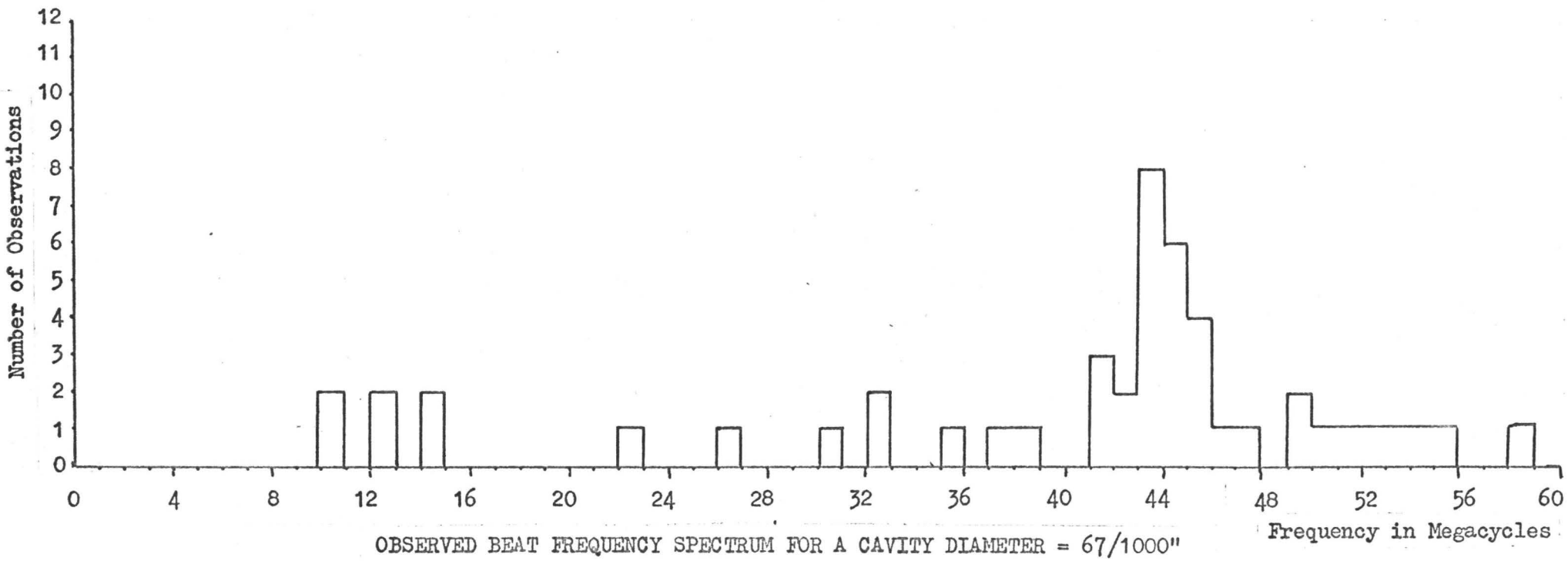


FIGURE 6.2

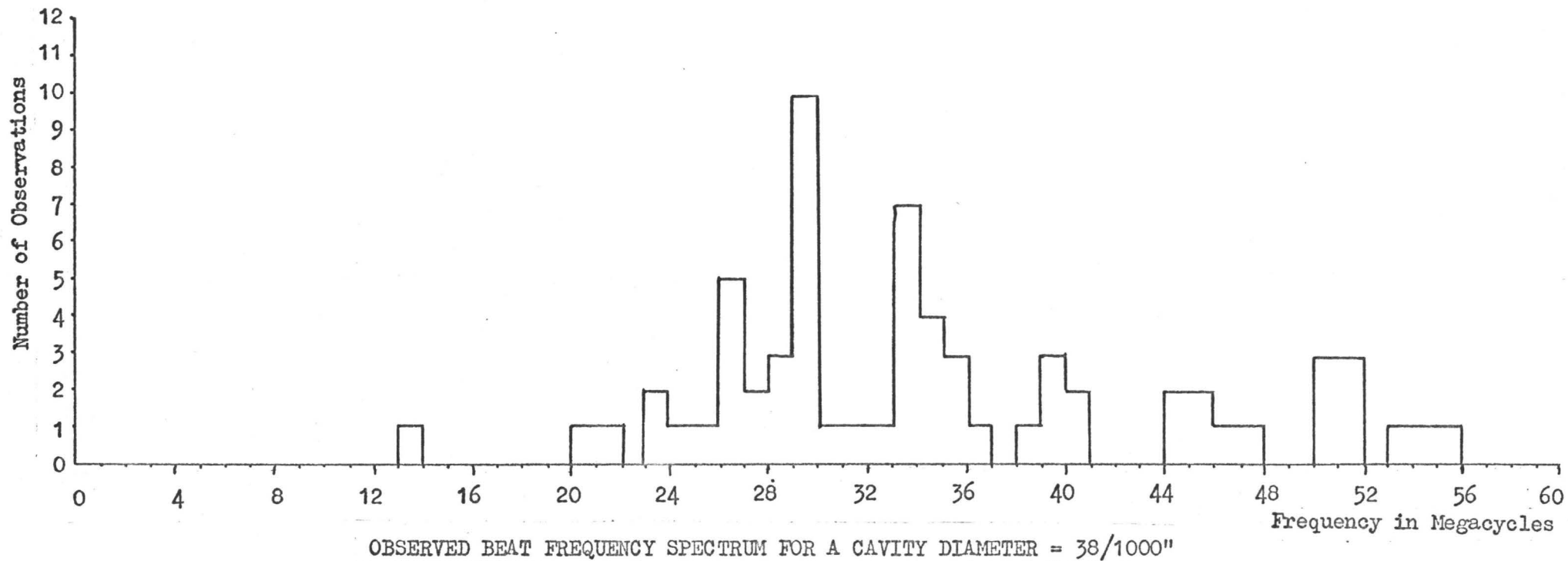


FIGURE 6.3

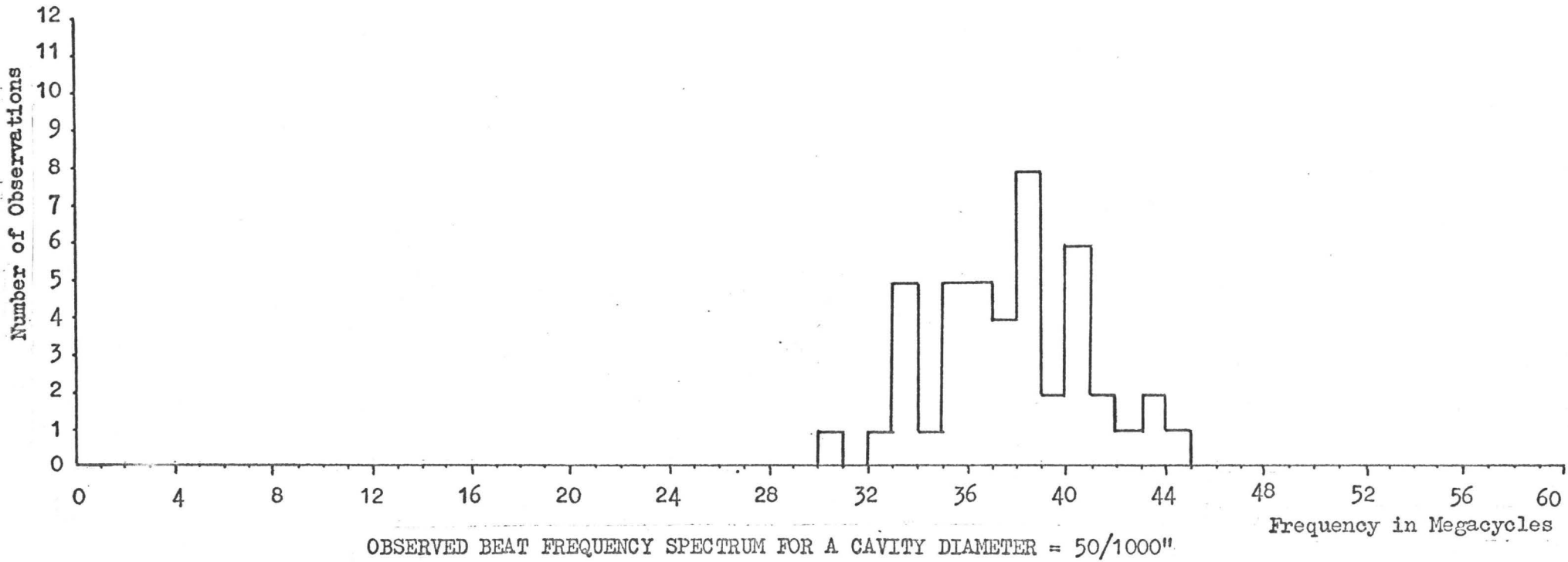
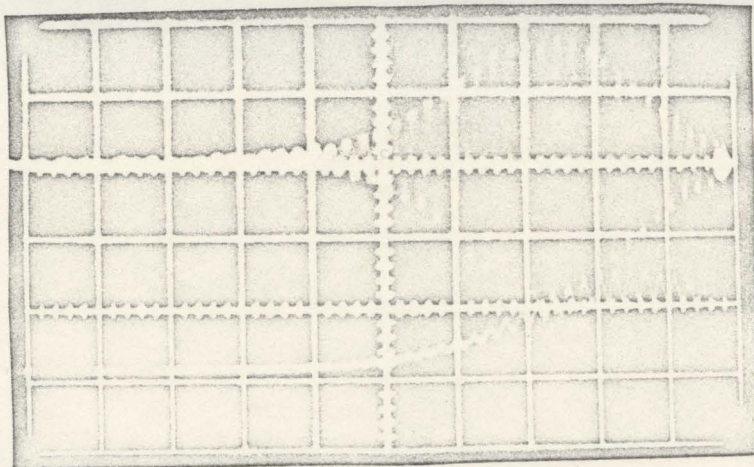
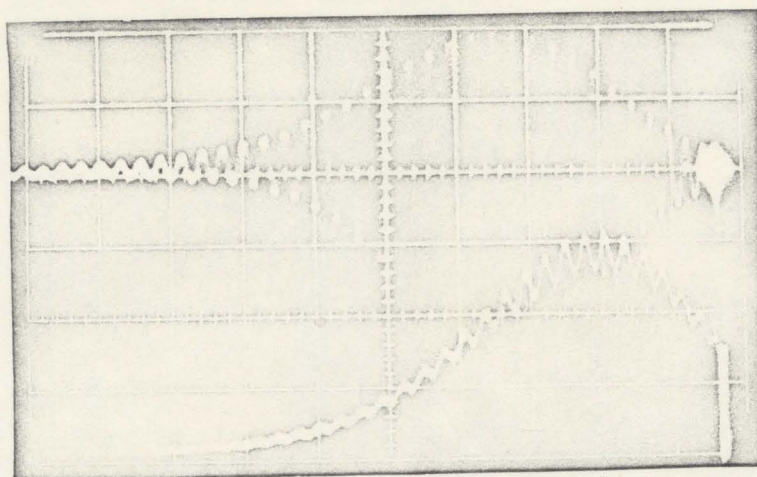


FIGURE 6.4



Cavity Diameter = 67/1000 "
Beat Frequency = 44 Mc
Temperature = 77 Degrees Kelvin
Pump Energy = 10 % Above Threshold

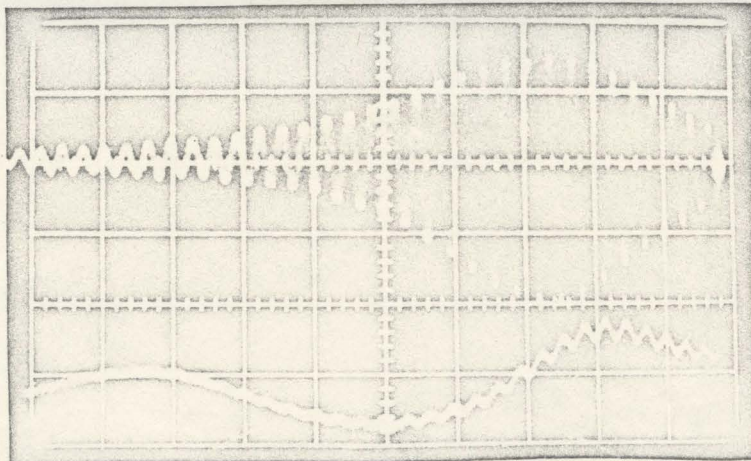


Cavity Diameter = 50/1000 "
Beat Frequency = 34.5 Mc
Temperature = 77 Degrees Kelvin
Pump Energy = 10 % Above Threshold

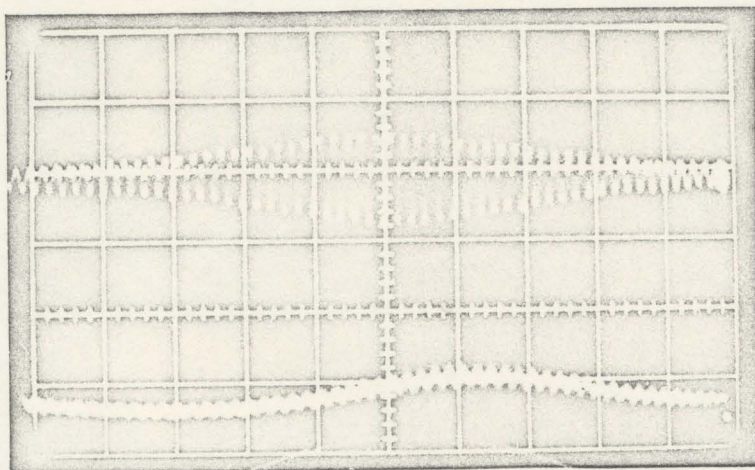
OSCILLOSCOPE TRACES SHOWING THE MODULATION CARRIED BY LASER RELAXATION

SPIKES

FIGURE 6.5



Cavity Diameter = $38/1000$ "
Beat Frequency = 32 Mc
Temperature = 77 Degrees Kelvin
Pump Energy = 10 % Above Threshold



Cavity Diameter = $34/1000$ "
Beat Frequency = 51 Mc
Temperature = 77 Degrees Kelvin
Pump Energy = 30 % Above Threshold

OSCILLOSCOPE TRACES SHOWING THE MODULATION CARRIED BY LASER RELAXATION

SPIKES

FIGURE 6.6

BEAT FREQUENCY IN MEGACYCLES

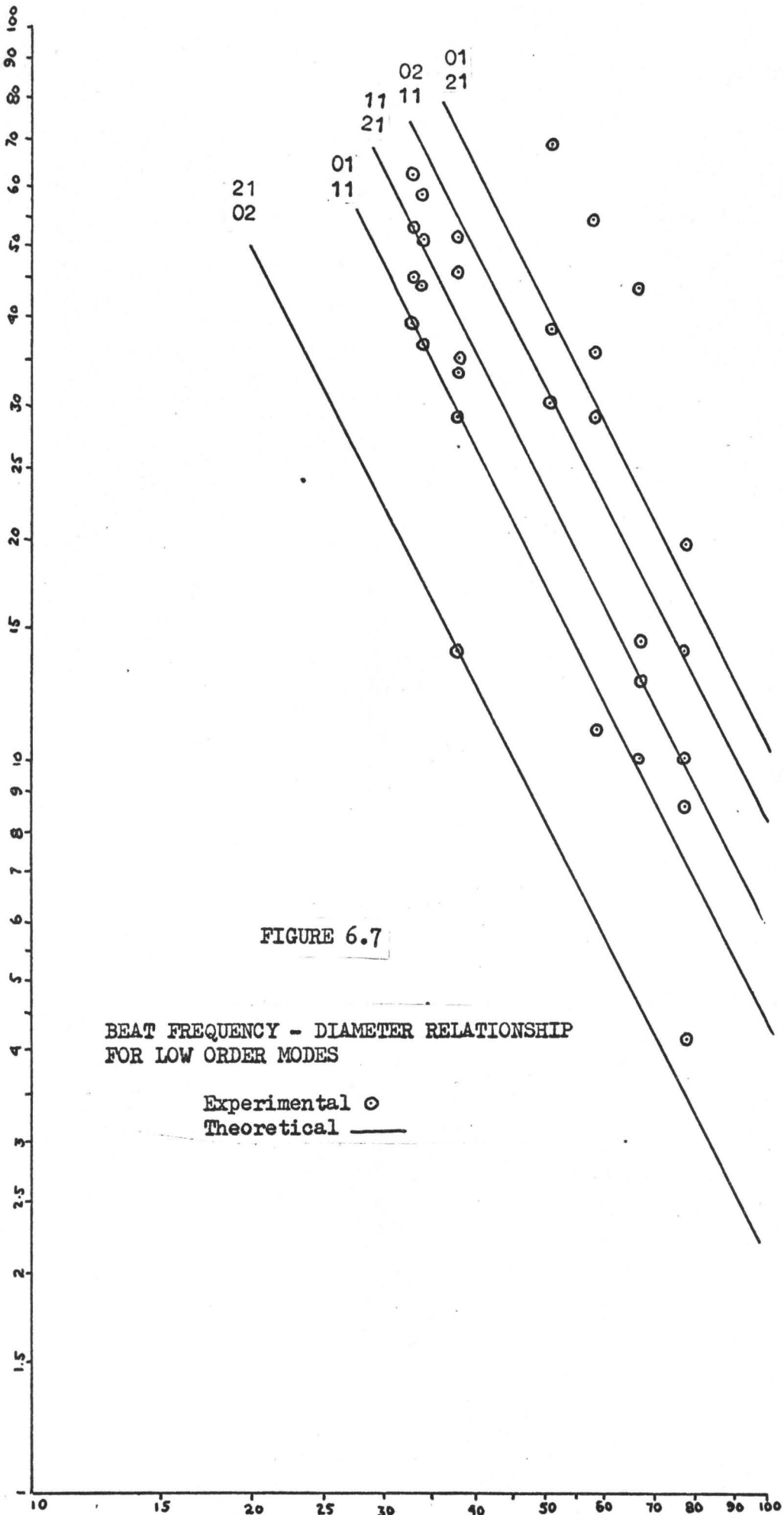


FIGURE 6.7

BEAT FREQUENCY - DIAMETER RELATIONSHIP FOR LOW ORDER MODES

Experimental ○
Theoretical —

DIAMETER OF CAVITY IN THOUSANDS OF AN INCH

the laser output and so any tendency for even a small peak to form far from the main peak must be interpreted as due to some other pair of modes going occasionally into oscillation.

The technique used to test the observed frequencies against those predicted by plane parallel resonator theory will now be outlined. Histogram plots were obtained for various resonator radii. The histogram related to a particular resonator radius was interpreted to contain only certain discrete frequencies. These discrete frequencies were plotted as a function of resonator diameter. The theoretical variation of beat frequency as a function of resonator diameter was plotted on the same graph (Figure 6.7). As can be seen from the results the agreement between experimentally observed and theoretically predicted beat frequencies is reasonable.

It should be pointed out that as the resonator radius is increased, the mode selectivity of the resonator decreases, and inhomogeneities in the ruby also play a more substantial role. It is only because a small Fresnel number is involved that plane parallel resonator theory can be applied to analyze the results. With the larger cavity radii employed, it was found that many more frequencies occurred within the observation range than with the smaller cavities. This is to be expected on the mode selectivity argument expressed above. Hence a significant histogram of a cavity whose diameter was 0.080 inch would need many more photographs than one of 0.040 inch diameter. The number of photographs that can be taken are limited by the lifetime of the silver deposit forming the cavity. It deteriorates quite rapidly, even at the low output

powers employed during the experiments. Deterioration of the silvered end reflectors was generally indicated by a lower density of mode production and consistent failure of the video amplifier to trigger the oscilloscope. This observation is explained in terms of resonator theory. When the silver deteriorates, it becomes dislodged from the ruby crystal end face. The result is a smaller distorted active resonator area, and hence modes that break into oscillation are expected to give rise to beat frequencies beyond the capabilities of the detecting system.

Very clean beats are observed often from the low Fresnel number cavities which were the subject of this study. They rise slowly in amplitude as a laser relaxation spike starts to build up and just as gradually disappear as the photon flux in the cavity decays, when the population inversion has been used up. The frequency stability of the beats is probably better than that measured with the available techniques. This implies a frequency stability over a relaxation spike width better than 3%.

On occasion, two beats are observed simultaneously. These appear generally as a slowly modulated beat frequency. It is not known whether they are due to two beats occurring with different axial indices, or to three modes of the same axial index beating in such a way as to produce two observable frequencies.

CHAPTER 7

CONCLUSIONS

Experimental evidence has been presented that shows that plane parallel resonator theory can be applied in describing the mode structure of a ruby laser. It is emphasized that such an application is only feasible for cavities whose Fresnel number is small, since only then can optical inhomogeneities of the medium of present state of the art ruby rods be neglected. Although the experimental evidence does not absolutely exclude all other possible explanations of the high frequency oscillation phenomena observed, it is felt that, in view of the measure of agreement between the experimental observations and those predicted from resonator theory, the oscillations are due to beats between transverse modes. Some type of mode selection occurs in ruby lasers operated at low temperature and low Fresnel number. If longitudinal mode selection narrows laser oscillation to one longitudinal mode, it is expected that oscillations in a single transverse mode can be obtained by lowering the Fresnel number of the cavity employed until the desired condition is obtained. Single mode operation is desirable in certain cases, such as in the experimental determination of the optical frequency doubling constants of certain solids. The availability of continually improving ruby laser rods may allow the absolute identification of the origin of the observed oscillations.

APPENDIX

A. Confocal Mirror Cavity Equation

The integral equation

$$y_n(x, \rho) = \lambda_n(\rho) \int_{-1}^1 e^{i\rho x x'} y_n(x', \rho) dx' \quad (1)$$

is known to satisfy the differential equation^{1,2,3,4}

$$(1-x^2) \frac{d^2 y}{dx^2} - 2x \frac{dy}{dx} + (A - \rho^2 x^2) y = 0 \quad (2)$$

A discussion of (2) is found in Flammer (p.12).

Construction of the functions $y_n(x, \rho)$ has been undertaken by Flammer as well as Stratton⁵. They have obtained expansions in terms of the Legendre Polynomials. The coefficients in the expansions have been calculated numerically from the difference equation for the coefficients $d_m^n(\rho)$ that arises when a series of the form

$$y_n(x, \rho) = \sum_{m=0}^{\infty} d_m^n(\rho) P_m(x)$$

is substituted into (2), and use is made of the recursion relations for the Legendre Polynomials.

It is the purpose of this note to show that the functions $y_n(x, \rho)$ can be constructed in a straight forward manner from (1) and that the functions so constructed are indeed those calculated by Flammer and Stratton from the differential equation, except for a normalization

constant. In particular Taylor series expansions of $d_m^n(p)$ and $\lambda_n(p)$ in ascending powers of p will be found for $y_0(x,p)$.

The method employed is similar to that used by Whittaker to construct the Mathieu Functions.

The fact that the integral equation (1) has only either even or odd solutions follows from the form of the equation. Thus, when we expand the Kernel of (1), we need only consider either its cosine or sine component when dealing with either even or odd solutions respectively.

We will expand the lowest order even mode to terms of order p^6 to indicate the method of procedure.

We define ⁶

$$a_{nm} = \int_{-1}^1 x^n P_m(x) dx = \frac{2^{m+1} n! \left(\frac{n+m}{2}\right)!}{\left(\frac{n-m}{2}\right)! (n+m+1)!} \quad \begin{array}{l} n \geq m \\ n-m \text{ even} \end{array}$$

$$= 0 \quad \text{otherwise.}$$

Notice that if $p \rightarrow 0$ in (2) the resulting equation is that satisfied by the Legendre Polynomials $P_n(x)$ with $A = n(n+1)$.

Thus, we expect that $\lim_{p \rightarrow 0} y_n(x,p) = P_n(x)$.

We put $p=0$ and let $y_n(x,0) = P_0(x)$ in (1).

Thus, we get $\lambda_0(0) = \frac{1}{2}$

Writing

$$\frac{1}{2\lambda_0(p)} = 1 + \alpha_2 p^2 + \alpha_4 p^4 + \alpha_6 p^6 + \dots \quad (3)$$

$$y_0(x,p) = P_0(x) + P_2(x) [\gamma_{12} p^2 + \gamma_{24} p^4 + \gamma_{26} p^6 + \dots] + P_4(x) [\gamma_{44} p^4 + \gamma_{46} p^6 + \dots]$$

$$+ P_6(x) [\gamma_{66} p^6 + \dots] + \dots \quad (4)$$

and substituting (3) and (4) into (1) we get

$$\left\{ P_0(x) + P_2(x) [\gamma_{22} P^2 + \gamma_{24} P^4 + \gamma_{26} P^6] + P_4(x) [\gamma_{44} P^4 + \gamma_{46} P^6] + P_6(x) [\gamma_{66} P^6] \right\} \left\{ 1 + \alpha_2 P^2 + \alpha_4 P^4 + \alpha_6 P^6 \right\} = \frac{1}{2} \int_{-1}^1 \left[1 - P^2 \frac{x^2 x'^2}{2!} + P^4 \frac{x^4 x'^4}{4!} - P^6 \frac{x^6 x'^6}{6!} \right] \left[P_0(x') + P_2(x') [\gamma_{22} P^2 + \gamma_{24} P^4 + \gamma_{26} P^6] + P_4(x') [\gamma_{44} P^4 + \gamma_{46} P^6] + P_6(x') [\gamma_{66} P^6] \right] dx'$$

Integrating and equating coefficients of equal powers of p

we arrive at the following three equations

$$\alpha_2 P_0(x) + \gamma_{22} P_2(x) = \frac{1}{2} \left[-\frac{x^2}{2!} a_{20} \right] \quad (5)$$

$$\alpha_4 P_0(x) + [\gamma_{22} \alpha_2 + \gamma_{24}] P_2(x) + \gamma_{44} P_4(x) = \frac{1}{2} \left[-\frac{1}{2!} x^2 \gamma_{22} a_{22} + \frac{x^4}{4!} a_{40} \right] \quad (6)$$

$$\alpha_6 P_0(x) + [\gamma_{22} \alpha_4 + \gamma_{24} \alpha_2 + \gamma_{26}] P_2(x) + [\gamma_{44} \alpha_2 + \gamma_{46}] P_4(x) + \gamma_{66} P_6(x) = \frac{1}{2} \left[-\frac{x^2 \gamma_{24} a_{22}}{2!} + \frac{x^4}{4!} \gamma_{22} a_{42} - \frac{x^6}{6!} a_{60} \right] \quad (7)$$

To assure that the above equations hold true for all x in $(-1,1)$ we make use of the orthogonality property of the Legendre

$$\text{Polynomials} \quad \int_{-1}^1 P_m(x) P_n(x) = \begin{cases} 0 & n \neq m \\ \frac{2}{2m+1} & n = m \end{cases}$$

Thus, we must have

$$2\alpha_2 = -\frac{1}{4} a_{20} \quad ; \quad \frac{2}{5} \gamma_{22} = -\frac{a_{20} a_{22}}{4} \quad ; \quad 2\alpha_4 = \frac{1}{2} \left[-\frac{1}{2!} a_{20} \gamma_{22} a_{22} + \frac{a_{40}^2}{4!} \right]$$

$$\frac{2}{5} [\gamma_{22} \alpha_2 + \gamma_{24}] = \frac{1}{2} \left[-\frac{1}{2!} a_{22} \gamma_{22} a_{22} + \frac{a_{42} a_{40}}{4!} \right]$$

$$\frac{2}{9} \gamma_{44} = \frac{1}{2} \left[\frac{a_{44} a_{40}}{4!} \right]$$

The equations arrived at from (7) are not written down to save space.

Notice that second order coefficients are just numbers. Knowing these it is a simple if tedious matter to calculate the fourth order coefficients, and so on to any order.

In particular, for $y_0(x,p)$ we can write the following general relations $\gamma_{nn} = (-1)^{n/2} \frac{2n+1}{4} \frac{1}{n!} a_{nn} a_{n0}$ (8)

$$\left[\gamma_{n,n+2} + \alpha_2 \gamma_{nn} \right] = \frac{2n+1}{4} \left[(-1)^{n/2} \frac{1}{n!} a_{nn} a_{n2} \gamma_{22} + \frac{(-1)^{\frac{n}{2}+1}}{(n+2)!} a_{n+2,0} a_{n+2,n} \right] \quad (9)$$

Flammer points out that since (2) is a second order differential equation there are two non-trivial independent solutions.

The convergent solution is given when

$$\lim_{m \rightarrow \infty} \frac{a_m^n(P)}{a_{m-2}^n(P)} = - \frac{P^2}{4m^2}$$

From (8) we see that at least for small values of P ($\gamma_{n,n+2} P^2 \ll \gamma_{nn}$)

$$\lim_{n \rightarrow \infty} \frac{a_n^0(P)}{a_{n-2}^0(P)} \doteq \lim_{n \rightarrow \infty} \frac{\gamma_{nn} P^2}{\gamma_{n-2, n-2}} = - \frac{P^2}{4n^2}$$

Thus, $y_0(x,p)$ as calculated above corresponds to the lowest order convergent even solution of (2).

That this is indeed the case has been verified by making numerical calculations using the coefficients in the table, and comparing the results with those of Flammer for the mode in question.

REFERENCES

- 1 E. G. C. Poole, Quart. J. Pure & App. Math. 49. 309 (1923)
- 2 E. L. Ince, "Ordinary Differential Equations", Dover 1956, pp 201
- 3 Whittaker and Watson, "Modern Analysis", Cambridge 1963, pp 426
- 4 Flammer, "Spheroidal Wave Functions", Stanford University 1957, pp 30, pp 56
- 5 Stratton, Morse, Chu, Little, Corbato, "Spheroidal Wave Functions", Technology Press of MIT Wiley 1956
- 6 Legendre, "Exercices de Calc. Int. II", pp 352

B. Approximate Solution to the Coupled Non-linear Differential Equations of Galanin

Galanin and co-workers (Optics and Spect. 14, January 1963, pp 86) proposed in 1962 two coupled non-linear differential equations to describe the time development of the coherent light output of some solid state optical masers. The equations they proposed are perhaps the simplest of many that have been put forth by several workers to describe the observed highly non-linear damped relaxation oscillations of the light output from solid state optical masers. The system of two equations takes into account stimulated emission, the decay of photons in a lossy cavity and the pumping rate.

It is not proposed here to justify the applicability of the equations to an oscillating laser system. It will simply be shown that the equations can be handled approximately using analytic methods. The approximations are realistic. The applicability of the approximate solutions to a particular laser system can be determined simply by observing the damped train of relaxation spikes from the system in question. It is an easy matter to decide qualitatively whether or not the damping of the spikes is strong. The magnitude of the damping determines whether or not the proposed approximate solutions can be applied to the system.

The equations proposed by Galanin are

$$\frac{dn}{dt} = E - bnp$$
$$\frac{dp}{dt} = bnp - \frac{p}{\tau_c}$$

where E, b, \mathcal{T}_c are constants. E is the pumping rate, b is a cross section for induced emission and is related to the Einstein B coefficient, \mathcal{T}_c is the photon cavity lifetime, n is the population inversion, p is the number of coherent photons in the cavity.

We are considering unit volume of laser material.

A change of variables puts the equations into a more useful form. We put

$$n = \frac{1}{b\mathcal{T}_c} + \sqrt{\frac{E}{b}} x, \quad p = \mathcal{T}_c E y, \quad t = \frac{1}{\sqrt{bE}} T$$

This transformation gives

$$\frac{dy}{dT} = xy \quad \frac{dx}{dT} = 1 - y - \mathcal{T}_c \sqrt{bE} xy$$

If the term $\mathcal{T}_c \sqrt{bE} xy$ is neglected with respect to $1 - y$ the phase plane trajectories of the system are given by

$$\int x dx = \int \left(\frac{1}{y} - 1\right) dy$$

or

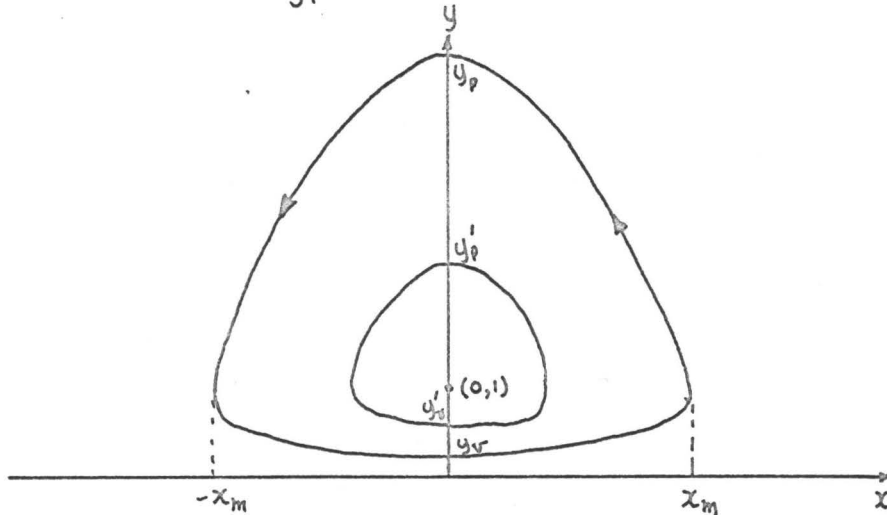
$$x^2 = 2 \left[\ln \frac{y}{y_p} - (y - y_p) \right]$$

This represents a family of closed trajectories in the x - y plane enclosing $(0,1)$. y_p is a parameter that gives the maximum value that y reaches. x takes on the extreme values

$$\pm x_m = \pm \sqrt{2} \sqrt{(y_p - 1) - \ln y_p}$$

The minimum value of $y = y_v$ is given by the solution of the equation

$$\ln \frac{y_v}{y_p} = y_v - y_p \quad \text{with } y_v \neq y_p$$



PHASE PLANE TRAJECTORIES OF THE APPROXIMATE SOLUTION TO THE COUPLED EQUATIONS

It can be seen from the coupled equations that the trajectories will be developed in an anti-clockwise direction as time increases. It is also evident that the term $\mathcal{I}_c \sqrt{b \epsilon} x y$ will curve the trajectories of the exact solution in such a way as to make them cross the approximate trajectories, always tending towards $(0,1)$. This in effect results in a continually decreasing y_p as time increases giving rise to damping of the output spikes. It is seen then that the exact trajectory will spiral into $(0,1)$ due to the action of the term $\mathcal{I}_c \sqrt{b \epsilon} x y$.

If during the time required for one complete cycle (ie. the time between two adjacent spike maxima) y_p does not change significantly then to all intensive purposes we can assume the functional

relationship between x and y to be given by the expression

$$x^2 = 2 \left[\ln \frac{y}{y_p} - (y - y_p) \right] \quad (1)$$

y_p does not change significantly of the two adjacent spike maxima are almost equal in magnitude.

The exact phase plane solution is given symbolically by

$$x^2 = 2 \left[\ln \frac{y}{y_p} - (y - y_p) - \tau_c \sqrt{bE} \int_{y_p}^y x \, dy \right] \quad (2)$$

A second order solution is obtained by substituting for in the integral of (2) using (1). This allows one to calculate successive values of y_p by putting

$$2 \left[\ln \frac{y}{y_p} - (y - y_p) - \tau_c \sqrt{bE} \int_{y_p}^y x \, dy \right] = 2 \left[\ln \frac{y}{y_p} - (y - y_p) \right]$$

The time development of x and y is then conceptually straight forward since an approximate functional relation is known between x and y .

Thus, for y we have $\frac{d \ln y}{d \tau} = x(y)$

and for x we have $\frac{d x}{d \tau} = 1 - y(x)$

These two later equations can be integrated approximately for certain ranges of variables in a simple manner. It is thus possible to compute the pulse train analytically.

REFERENCES

- 1 Schawlow, A. L., "Fine Structure and Properties of Chromium Fluorescence in Aluminum and Magnesium Oxide", Advances in Quantum Electronics, Columbia University Press (1961)
- 2 Evtuhov, V., and Neeland, J. K., Appl. Opt. 1, 517 (1962)
- 3 Dayhoff, E. S., Proc. IRE (corres.) 50, 1684 (1962)
- 4 Stickley, C. M., Appl. Opt. 2, 855 (1963)
- 5 Hughes, T. P., and Young, K. M., Nature 196, 332 (1962)
- 6 Clark, G. L., Rideway, S. L., Wuerker, R. F., and York, G. M., "High Speed Photographic Study of the Structure of Ruby Laser Emissions", Space Technology Laboratories Technical Report (1962)
- 7 Stickley, C. M., Proc. IEEE 51, 848 (1963)
- 8 Boyd, G. D., and Gordon, J. P., Bell Syst. Tech. J. 40, 489 (1961)
- 9 Flammer, C., Spheroidal Wave Functions, Stanford University Press, Palo Alto, California (1957)
- 10 Birnbaum, G., Optical Masers, Academic Press, New York (1964)
- 11 Mallory, W. R., Proc. IEEE 51, 850 (1963)
- 12 Fox, A. G., and Li, T., Bell Syst. Tech. J. 40, 453 (1961)
- 13 Bergstein, L., and Schachter, H., J. Opt. Soc. Am. 54, 887 (1964)
- 14 Stickley, C. M., J. Appl. Opt. 3, 967 (1964)

REFERENCES (CONTINUED)

- 15 Snitzer, E., "Optical Dielectric Waveguides", Advances in Quantum Electronics, Columbia University Press (1961)
- 16 Sommer, H. S., Proc. IEEE 51, 140 (1963)
- 17 Lucovsky, G., Lasser, M. E., and Emmons, R. B., Proc. IEEE 51, 166 (1963)